

APPLICATION OF
HOLOGRAPHIC INTERFEROMETRY TO THE
EXTERIOR BALLISTIC FLOW FIELD IN THE
MUZZLE ENVIRONMENT OF A
TWENTY MILLIMETER CANNON

Robert Gene Bettinger

DUDLEY KNOX LIBRARY
NAVAL POSTGRADUATE SCHOOL
MONTEREY, CALIFORNIA 93940

NAVAL POSTGRADUATE SCHOOL

Monterey, California



THESIS

APPLICATION OF
HOLOGRAPHIC INTERFEROMETRY TO THE
EXTERIOR BALLISTIC FLOW FIELD IN THE
MUZZLE ENVIRONMENT OF A
TWENTY MILLIMETER CANNON

by

Robert Gene Bettinger

June 1975

Thesis Advisor

Daniel J. Collins

Approved for public release; distribution unlimited.

T167529

REPORT DOCUMENTATION PAGE		READ INSTRUCTIONS BEFORE COMPLETING FORM
1. REPORT NUMBER	2. GOVT ACCESSION NO.	3. RECIPIENT'S CATALOG NUMBER
4. TITLE (and Subtitle) Application of Holographic Interferometry to the Exterior Ballistic Flow Field in the Muzzle Environment of a Twenty Millimeter Cannon		5. TYPE OF REPORT & PERIOD COVERED Engineer's Thesis June 1975
7. AUTHOR(s) Robert Gene Bettinger		6. PERFORMING ORG. REPORT NUMBER
9. PERFORMING ORGANIZATION NAME AND ADDRESS Naval Postgraduate School Monterey, California		8. CONTRACT OR GRANT NUMBER(s)
11. CONTROLLING OFFICE NAME AND ADDRESS Naval Ordnance Station, Indian Head, Md.		10. PROGRAM ELEMENT, PROJECT, TASK AREA & WORK UNIT NUMBERS 4-0029
14. MONITORING AGENCY NAME & ADDRESS (if different from Controlling Office)		12. REPORT DATE June 1975
		13. NUMBER OF PAGES
		15. SECURITY CLASS. (of this report) Unclassified
		15a. DECLASSIFICATION/DOWNGRADING SCHEDULE
16. DISTRIBUTION STATEMENT (of this Report) Approved for public release; distribution unlimited.		
17. DISTRIBUTION STATEMENT (of the abstract entered in Block 20, if different from Report)		
18. SUPPLEMENTARY NOTES		
19. KEY WORDS (Continue on reverse side if necessary and identify by block number) Holographic Interferometry Exterior Ballistic Flow		
20. ABSTRACT (Continue on reverse side if necessary and identify by block number) The technique of holographic interferometry was applied to the study of the gas core characteristics in the muzzle environment of a 20 mm cannon. Experimental measurements were made of the muzzle velocity and of gas core pressures at the cannon breech to verify prediction of these parameters in a numerical technique using standard hydrodynamic equations. Holographic interferograms were made of the projectile and its associated flow field during launch.		

Application of Holographic Interferometry
to the
Exterior Ballistic Flow Field in the Muzzle Environment
of a
Twenty Millimeter Cannon

by

Robert Gene Bettinger
Lieutenant, United States Navy
B.S., Case Institute of Technology, 1964

Submitted in partial fulfillment of the
requirements for the degree of

AERONAUTICAL ENGINEER

ABSTRACT

The technique of holographic interferometry was applied to the study of the gas core characteristics in the muzzle environment of a 20 mm cannon. Experimental measurements were made of the muzzle velocity and of gas core pressures at the cannon breech to verify prediction of these parameters in a numerical technique using standard hydrodynamic equations. Holographic interferograms were made of the projectile and its associated flow field during launch.

TABLE OF CONTENTS

LIST OF SYMBOLS-----	6
I. INTRODUCTION-----	8
II. HOLOGRAPHIC INTERFEROMETRY-----	10
III. EXPERIMENTAL LAYOUT-----	15
A. GENERAL PHYSICAL ARRANGEMENT-----	15
B. OPTICAL SYSTEM-----	16
C. BARREL INSTRUMENTATION-----	19
IV. FIRING SEQUENCE-----	21
V. HOLOGRAPHIC FILM AND PROCESSING TECHNIQUE----	24
VI. RECONSTRUCTION-----	26
VII. COMPUTER PROGRAM FOR FLOW PARAMETER PREDICTION-----	28
VIII. HOLOGRAPHIC RESULTS-----	31
IX. COMPARISON OF ANALYTIC AND EXPERIMENTAL RESULTS-----	35
X. SUMMARY AND RECOMMENDATIONS-----	37
FIGURES-----	38
APPENDIX A: GUN PROJECT COMPUTER PROGRAM-----	65
A. PROGRAM LISTING-----	69
B. INPUT FORMAT-----	104
LIST OF REFERENCES-----	109
INITIAL DISTRIBUTION LIST-----	111

LIST OF SYMBOLS

<u>Symbol</u>	<u>Definition</u>
A	cross-section area
C_o	constant specifying thickness of shock region
d	projectile nose diameter
E	specific internal energy
j	mass point number
M	mass
n	cycle number
p	pressure
q	artificial viscosity
t	time
u	velocity
V	specific volume
x	Eulerian position
Δs	shock standoff distance
ρ	density

ACKNOWLEDGEMENT

The author wishes to express his appreciation to Dr. D. J. Collins for his invaluable guidance and considerable personal involvement during the course of this study, to Dr. D. W. Netzer for his constructive suggestions and counsel, and to the technical staff of the Department of Aeronautics, particularly P. Hickey and N. Leckenby, for their assistance in the construction and operation of the equipment of this investigation.

This work was sponsored by the U. S. Naval Ordnance Station, Indian Head, Maryland under Project Number 4-0029.

I. INTRODUCTION

A thorough knowledge of the physical characteristics of the internal gas flow field is essential in ballistic design. The flow field that is created and exists ahead of the projectile external to the barrel of any ballistic device also plays an important role in the performance of the projectile. The projectile must traverse this unsteady flow field prior to entering a freestream environment and may therefore have its trajectory altered by this field. Projectile design then may be highly dependent on an understanding of the properties of this flow field existing at the muzzle face. Design of muzzle devices intended to control this environment must also stem directly from knowledge of these characteristics.

A number of experimental and theoretical studies of this external field have been conducted and have shown it to be a complicated structure of mixed supersonic and subsonic flow with a network of shock and expansion areas.

Oertel [Ref. 1] has examined the development of the field using a muzzle flow simulator and a multiple pulse laser to produce a sequence of laser interferograms. The luminosity of this field has been studied by Schröder and Klingenberg [Ref. 2] using small caliber guns of low muzzle velocities with spectroscopic techniques. Theoretical studies have included the development of a numerical scheme which simulates

the blast field and introduces the projectile into the field to determine the effects of the field on the projectile [Ref. 3].

Holographic interferometry has been successfully applied in the study of a wide range of aerodynamic flow problems because of its capability of allowing the investigator to store transient wavefront information for later recall. This aspect of the technique is particularly appealing to the inherently short duration ballistic flow fields. Recent advances in the area of fringe data reduction have greatly reduced the time and energy involved in obtaining density distributions from the interferometric data.

This investigation was conducted in three separate segments:

1. Application of the holographic interferometry technique to the study of the gas core characteristics in the muzzle environment of a 20-millimeter cannon.
2. Experimental measurement of the gas core temperatures and pressures at the breech of the cannon using high frequency pressure transducers and thermocouples, and muzzle velocity measurements taken with a precision chronograph triggered by projectile passage through optical velocity screens.
3. Analytical prediction of muzzle velocities and pressure histories using standard inviscid theory.



II. HOLOGRAPHIC INTERFEROMETRY

The utility of holography as an interferometric tool was recognized in the mid-1960's, shortly after the introduction of the laser as a coherent light source for wavefront reconstruction. Interferometry is the technique of combining two beams of coherent light, that is, beams with a well-defined and non-varying phase relationship. The resulting light and dark interference bands or fringe pattern may be used to measure displacements, density variations and wave characteristics. The use of holography greatly enhances the interferometric technique. The unique property of holography is that it permits photographic storage of a transitory wavefront, which is then available for later reconstruction at the convenience of the investigator. This property then permits interferometric comparison of beams of short duration or beams not simultaneously available.

Two techniques of holographic interferometry are of particular importance. The first of these is called "real time" interferometry. Figure 1 provides an illustration of this technique. In this process, a hologram is first produced of the subject in its unperturbed state. After processing, the photographic plate containing the hologram is replaced in its exact exposure location relative to the original subject and all optical equipment. The subject is then placed in its perturbed state. The hologram and subject are then re-illuminated with the

original subject and reference wavefronts. The original undisturbed subject wavefront is reconstructed and interferes with the perturbed subject wavefront, producing a fringe pattern. Changes in the fringe pattern resulting from varying perturbations may then be continuously monitored.

The second method with numerous applications is the double exposure technique. The hologram is exposed twice prior to processing, with the subject in both the perturbed and unperturbed states. Upon reconstruction, both waves are simultaneously reproduced and interfere, creating the desired fringe pattern. This technique has several advantages over the "real time" technique. More flexibility of observation is attainable and distortion due to emulsion shrinkage is eliminated. Additionally, optical components of lower quality may be used, since the double exposure cancels optical component defects. Unfortunately, the technique permits analysis of only a single distorted state per hologram.

If the optical path between exposures is unchanged, and no disturbance is introduced into the field, the resultant fringe pattern is referred to as the "field of infinite fringe" and consists of a single fringe of infinite width. With the disturbance introduced on the second exposure, small phase shifts in the subject field produced by changes in the optical path length result in a limited number of fringes. If a slight displacement or translation of the scene beam is initiated between exposures, a

framework of sharply defined parallel fringes of selectable spacing is introduced into the hologram. This "finite fringe field" represents lines of constant differences in optical path length. The spacing and clarity of the finite fringe pattern is dependent on the amount of translation or rotation of the scene beam. A quantitative relationship between fringe spacing and rotation or displacement is provided by Floyd & Collins [Ref. 6]. If the subject is then perturbed for the second exposure, density gradients are indicated by fringe shifts often more easily analyzed than the infinite fringe field, particularly for small gradients. Measurement of fringe shifts then allows determination of the density field.

The two most commonly employed schemes for illuminating the object are diffuse lighting and non-diffuse or direct lighting, each of which are illustrated in Figure 2.

Direct illumination is particularly useful for flow visualization of two-dimensional and axi-symmetric flow fields and is generally simpler to set up and use, requiring less intensity for subject illumination. When a diffusing glass is placed in front of the subject, significant changes occur. If the subject is a phase object, each point in the field receives illumination from an infinite number of directions. Thus, each point on the hologram plate receives scattered light from every point in the subject. The entire subject may then be viewed by illuminating any part of the hologram. Different views of the subject are

obtainable by re-illuminating different portions of the hologram plate with the reference beam. Three-dimensional diffusely reflecting objects scatter light in a similar manner as the diffusing glass and thus the glass may be omitted when producing holograms of these subjects. Three-dimensional images of opaque objects may be reconstructed and photographed from different viewing angles using a single hologram.

Diffusely illuminated subjects produce holograms with light field backgrounds which are easier to view than the dark background of direct illumination. A problem arising with diffuse lighting is that the loss of spatial coherence between the interfering waves often causes localization of the fringe system in a plane other than that of the subject. If this separation is too large, it may become necessary to use a lens system with a large depth of field to image both the subject and fringes. Such a system may place limits on the resolution obtainable.

A primary consideration in the technique of holographic interferometry of flow fields is the source of coherent light. In order to maintain the stability of the flow field necessary for high resolution holograms, it becomes necessary to shorten exposure times to the point where changes in the optical path length are restricted to less than the wavelength of light.

The Q-switched pulsed ruby laser has proved to be an excellent light source for these applications. It provides the high power

necessary to expose the plate in a time frame suitable for freezing the motion of the flow field. The wavelength of this laser is compatible with certain commercially available holographic film plates. An additional advantage of this system is that it provides a coherence length of approximately 1 meter, thus eliminating the need to precisely match the path lengths of the reference and scene beams. The short pulse length of this laser makes it mandatory to provide a secondary continuous wave laser beam coincident with the ruby beam for alignment of the optical components. A description of the common technique for placing these beams in coincidence is available in Ref. 7.

III. EXPERIMENTAL LAYOUT

A. GENERAL PHYSICAL ARRANGEMENT

The 20-mm cannon was mounted muzzle end facing outward on a steel rocket test stand within a test cell at the Naval Postgraduate School Rocket Laboratory. These test cells measured 12' x 17' with reinforced concrete walls 12 inches thick. The barrel was secured horizontally to the test stand via two steel mounts at a height of $6\frac{1}{2}$ inches from the stand to the barrel centerline. Two large wooden tables were constructed the length of the test stand and placed parallel to it, one on each side for housing the optical system. These tables were rigidly fastened together and isolated from the test stand to maintain stability and minimize vibrational effects from the cannon blast. Plywood covers were constructed for the tables to protect the optical components and provide the necessary light shield for the holography. The tops to these plywood covers were hinged to allow easy access to the optical components. The general layout of the cell can be seen in Figure 3.

The electrical firing mechanism for the cannon was placed on the test stand at the breech end. All controls for firing the cannon were located remotely in a control room directly behind the back wall of the test cell. The projectile was fired into a bullet trap located 13 feet outside the cell. The trap was designed for the bullet to first impact

on an 18" x 18" x 1½" armor plate tilted 45° from the path of the projectile. This first contact shattered the shell and deflected the fragments into a steel-encased sand trap measuring 5' x 5' x 2½'. The sand trap itself was again shrouded with sand bags for additional safety. The entire trap was housed in a steel turret for a 5" gun mount measuring approximately 15' x 20' x 10'. Figure 4 shows the front of the turret and projectile path.

The ruby laser and all of its components were placed in the test cell adjacent to the cannon. This was done partly for space considerations and also for protection of the ruby laser components. The rail containing the laser cavity was mounted on a specially constructed table and faced normal to the wall separating the cells. A 2-inch hole was drilled through the concrete wall to allow beam passage. The cell was provided with a water source for the laser head and output etalon cooling system. The laser was equipped with a remote control unit so that it could be fired either from the test cell or the remote control room.

B. OPTICAL SYSTEM

The holographic optical schematic is shown in Figure 5. The laser system used for the actual holography was the Korad K-1 pulsed ruby laser. This system is capable of delivering high power, single transverse mode output in the Q-switched mode of operation. A Pockels cell was used to provide the Q-spoiling necessary for peak

power output. When operated in the TEM_{00} mode, typical values for pulse energy and pulse width are 0.050 joules over 20 nanoseconds, yielding a peak power of 2.5 megawatts. The output beam is approximately 2 mm in diameter with a wavelength of $6943 \overset{O}{\text{\AA}}$ and a coherence length in excess of one meter. The laser head was equipped with a high optical quality holographic ruby rod. Figure 6 provides a photographic view of the laser installation.

After first passing through the holes in the wall and plywood cover, the beam then passed a narrow-band filter which served to remove the undesired light from the Xenon flash tube. After next passing a series of neutral density filters used to control intensity, the beam then contacted a 2-inch round beam splitter which divided it into two wavefronts of approximately equal intensities. The subject beam was reflected down the centerline of a 2.5 meter optical bench through a series of expanding, collimating lenses to mirror #1. These lenses were designed to expand the subject beam to a size compatible with the field of interest and the 4" x 5" hologram plate. Mirror #1 was secured to a precision gimbal mount which allowed rotation about both the vertical and horizontal axes. This mount provided the precise beam rotation necessary to produce the finite fringed field for interferometry. Mirror #1 directed the beam through the test section and a dual grid system in a direction normal to the axis of the cannon.

The beam was then reflected from mirror #2, which directed it along a 1.5 meter optical bench through a set of imaging lenses with

a focal length of 22 inches. The purpose of this set of lenses was to image the test section closer to the hologram plate providing a sharper image with greater fringe contrast. This set of lenses converged the beam to a point at which a second narrow-band filter was placed to remove the flash from the muzzle blast. The beam then passed to mirror #3 which directed it to the hologram plate.

After passing the beam splitter, the reference beam contacted mirror #4 on a 2.0 meter optical bench which allowed adjustment of the reference beam path length to that of the subject beam. From mirror #5 the beam was directed to the hologram plate through two series of expanding-collimating lenses which enlarged the beam to approximately a 4" diameter at the plate. All mirrors in the system were provided with screw type adjustments for vernier-scale movement about their horizontal and vertical axes, thereby greatly simplifying alignment procedures.

The optical benches were bolted to the tables on specially designed crossfeet which allowed the benches to be leveled with two knob adjustments provided on each crossfoot.

For alignment the system was equipped with a Coherent Radiation 3 milliwatt helium-neon continuous wave laser. This laser was mounted on a stand perpendicular to the axis of the ruby laser cavity. By placing a mirror at a 45° angle in the ruby laser cavity, this CW beam could be placed in coincidence with the ruby laser beam.

The overall performance of the optical system was measured through the use of the USAF 1951 resolution test target (Figure 26). The target was placed in the test section and a hologram taken. Examination of the reconstruction of this hologram (Figure 27) reveals a minimum resolution of 3.5 lines per mm which is more than adequate for the fringe shift measurements necessary in the conduct of the interferometry. Figure 7 is a photographic view of the optical arrangement.

C. BARREL INSTRUMENTATION

For measurement of the pressure-time history at the breech end, the barrel was equipped with Kistler 607A pressure transducer installed $5\frac{1}{2}$ inches from the breech end of the barrel. This location was just ahead of the tip of the projectile prior to firing. The signal from the transducer was passed to a Kistler Model 504 Universal Charge Amplifier in the control room and then displayed on a Textronix storage oscilloscope.

Gas core temperature measurements were made at the breech with a special Nanmac tungsten-rhenium thermocouple mounted directly opposite the Kistler transducer. The output from this thermocouple was displayed on a Hewlett-Packard OS 209 (P) oscilloscope.

For muzzle velocity measurements, the projectile was fired through two Oehler Model 55 Ballistic Velocity Screens placed in the path between the muzzle and the sand trap. These screens can be seen in Figure 4. As the bullet passed through each screen, a 12-volt pulse

with an adjustable 2-8 millisecond pulse length was produced and sent to an Oehler Model 21 Chronograph. These pulses provide start and stop signals for the chronograph. This provides a time of passage between the two screens. The screens are placed a known distance apart and thus an average velocity between the two can be calculated. These velocities are tabled for various screen separations. It was found that the first screen had to be placed at least 4 feet from the muzzle to prevent the blast from pre-triggering the screen prior to projectile passage. Figure 8 is a photograph of the control room instrumentation including the fire control panel.

IV. FIRING SEQUENCE

After optical system alignment and warm-up of all electrical components, the test cell was closed and a hologram plate installed in its holder. The laser was fired from its direct control for the first plate exposure of the unperturbed field. This first exposure creates the hologram of the static test section which will later be used to interfere with the second hologram of the flow field. For the finite fringe holograms, mirror #1 was then rotated to produce the desired fringe field for the reconstruction process. Mirror #1 mount was equipped with two micrometer adjustments which provided 20 arc seconds of beam rotation for each unit of micrometer movement. Beam rotation of approximately 100 arc seconds between shots provided the fringe field desired. For infinite fringe holograms mirror #1 was not moved.

After producing the reference hologram the cannon was loaded. The individual who was loading the cannon and connecting the firing mechanism carried with him a safety key which breaks the firing circuit at the control panel to prevent accidental firing prior to his clearing the test area. The laser was then charged remotely from the control room and a horn was sounded to provide final warning of the impending shot. The firing sequence was then initiated. A schematic of this sequence is shown in Figure 9.

While the laser capacitor bank was charging, the safety key was installed in the fire control panel and power supplied to the firing mechanism. When the laser was ready, the firing mechanism capacitors were charged and the cannon then fired. The process could be observed through two glass viewing windows connecting the control room and the test cell.

To provide accurate timing for firing the laser coincident with projectile passage through the test area, it was necessary to use the pulse from the Kistler transducer to initiate the laser firing sequence. After a number of measurements, it was found that for the studies outside the barrel, projectile passage through the test area occurred at approximately 1600 microseconds after the triggering of the Kistler. The laser system has an inherent delay of about 1020 microseconds between discharge of the capacitor bank and lasing action with Pockels cell Q-switching. Additionally, the output voltage from the Kistler charge amplifier was not sufficient for triggering the laser. It was therefore necessary to delay and increase the voltage of the Kistler pulse to provide an accurate reliable trigger for the laser system. To do this, the Kistler pulse was displayed on a Textronix storage oscilloscope and simultaneously used as an input to a Hewlett-Packard USM-310(V) signal modulator. This unit permits the input of a variable signal delay which was changed periodically to adjust to point of exposure on the projectile. The delayed Kistler output was routed through an

ILC PG-10 pulse generator which provided the voltage necessary to trigger the laser.

Additionally, two electronic timers, a Monsanto Model 101 B and a Dynasciences CP-929 were integrated into the system at various locations to provide checks on intervals of interest. These are shown in typical locations in the firing sequence schematic.

After firing, the test cell was closed and the hologram plate removed for processing. The armor plate was checked for damage and repositioned when necessary. The cannon was unloaded and the barrel was periodically cleaned with a standard 20-mm bore brush. The pressure and temperature traces were photographed with a Polaroid C-5 oscilloscope camera.

V. HOLOGRAPHIC FILM AND PROCESSING TECHNIQUE

The wavelength of the coherent light source used in the holography is 6943 \AA° . It was desirable to use a photographic emulsion with narrow-band sensitivity centered in this region of the spectrum to minimize the effect of extraneous light leakage into the system. The most suitable commercially available emulsion for this purpose was found to be Agfa-Gevaert 10E75 holographic plates. This film has a resolution capability of 2800 lines per mm which is approximately the maximum required film resolution for transmission holograms produced with 6943 \AA° light. A spectral sensitivity curve for this emulsion may be found in Ref. 4.

Processing of the exposed hologram plates consisted of a five-minute bath in Kodak D-19 Developer followed by five minutes in a standard fixer. The plate was then washed for five minutes in flowing water and then allowed to air dry prior to reconstruction.

It was not possible to control time of exposure for these plates while using the 20-nanosecond ruby pulse. Therefore, exposure was controlled by using a suitable combination of neutral density filters in the beam to produce the intensity desired at the hologram plate.

For the double pulsed holograms a problem was encountered due to the fact that the projectile was not in the field for both exposures as is normally the case when utilizing this technique to observe flow

fields around opaque objects. For single exposure holograms the bullet appears as a dark object in a light background, while for double exposure holograms the bullet was a light object on a light background. This lack of contrast was improved appreciably by halving the intensity of the first exposure. This provided a grey background for the bullet upon reconstruction, while yielding good fringe contrast.

VI. RECONSTRUCTION

In reconstruction of the holograms, two different techniques were employed using different sources of coherent light for the reconstructing reference wave. For the first of these, illustrated in Figure 10, a 15-milliwatt Spectra-Physics continuous wave, helium-neon laser was used for the reconstructing wave. This laser was equipped with an integral lens system which produced a 50-millimeter collimated beam. This beam was expanded and collimated with a secondary set of lenses to the approximate size of the hologram plate. The converging real image was then photographed with a single lens reflex 35-millimeter camera, using Kodak Panatomic-X (ASA 32) fine grain black and white film.

The second reconstructing procedure used is illustrated in Figure 11. A one-watt continuous wave argon laser was employed to reconstruct overexposed holograms requiring a more intense reference beam. To minimize the possibility of accidentally viewing the powerful reference beam during photography, the reconstructed scene beam was reflected away from the reference beam with a high quality first surface mirror. As suggested by Trolinger [Ref. 11], the actual imaging lens used in the construction of the hologram was placed in the reconstructed scene beam to eliminate spherical aberrations produced by this lens during construction. This lens then served to recollimate the scene

beam. In practice, little or no improvement was observed in the quality of the reconstructed beam. Thus this lens was not used in the first technique.

The real image was again photographed with the single lens reflex camera and Kodak film.

VII. COMPUTER PROGRAM FOR PREDICTION OF FLOW PARAMETERS

The computer program used for the prediction of the muzzle velocity and pressure history of the flow field was an adaptation of a program developed at the Naval Ordnance Laboratory to analyze the performance of hypervelocity model launchers [Ref. 8]. The analysis was essentially a one-dimensional, Lagrangian scheme in which the field was divided into six regions, each of which then was subdivided into zones. Each region had specified its own equation of state which, depending upon the material characteristics of the region, could be either solid, ideal, or non-ideal gas equations. At the interface of each zone were inserted mass points, each of which was assumed to consist of one-half of the mass of the adjacent zone. The analysis successively applied the hydrodynamic equations in finite difference form to each mass point over the time interval of interest. The method employed was the "q" method of Von-Neuman and Richtmyer [Refs. 9 and 13].

The equations applicable to the scheme were the following:

Isentropic Flow energy equation:

$$\frac{\partial E}{\partial t} = -(p + q) \frac{\partial V}{\partial t}$$

Equation of motion:

$$\frac{\partial u}{\partial t} = - \frac{\partial (p + q)}{\partial x} \frac{1}{M} A(x)$$

Equation of state:

$$p = p(E, V)$$

with

$$M = \int^x \rho(x) A(x) dX$$

$$q = \begin{cases} \frac{C_o^2}{V} \left(-\frac{\partial u}{\partial j} \right), & \frac{\partial u}{\partial j} < 0 \\ 0, & \frac{\partial u}{\partial j} \geq 0 \end{cases}$$

The artificial viscosity term "q," which was added to the pressure term in the energy and motion equations, essentially spreads variable changes created by the shock over a finite region. This facilitates computation by allowing the equation variables to be continuous across the shock. The constant C_o permits adjustment of this shock "thickness."

For computation purposes these equations were written in finite difference form. Initial values of E_o , p_o , and V_o are provided for each region. Stability was maintained during the process by recalculating a new time increment for every cycle in the process.

During each cycle, the pressure at each mass point was calculated using the equations of state and energy. From the pressure differential at these interfaces the acceleration and velocity of each mass point were obtained using the equation of motion.

Required data inputs included initial temperatures, pressures, and molecular weights for each region, along with a series of variables

describing the geometry of each region. Additional inputs describing burning characteristics were required for each region containing powder.

The program was written in FORTRAN and a listing along with the input format is given in Appendix A.

VIII. HOLOGRAPHIC RESULTS

Considerable trial and error was involved in the initial attempts to capture the projectile and its associated flow field at the muzzle of the barrel. The optics of the system were initially designed primarily for investigation of the interior flow behind the projectile and thus the available size of the scene beam was limited. The average view of the test section was circular of 4-cm diameter centered 2.5 cm outside the muzzle. Initially a barrel-mounted dual grid system (one grid on each side of the test section) was installed on the barrel. These grids were removed and replaced with a central vertical wire for viewing orientation when it was discovered that grid movement due to the blast introduced undesirable noise into the system for the double-pulsed holography.

Prediction of the pulsing instant of the Q-switched laser was reliable to within ± 10 microseconds. The time of projectile passage through the test section after triggering the transducer varied by as much as 50 microseconds. This variability was reflected in the range of projectile velocities obtained from the velocity screens and was probably a result of differences in powder charge and projectile weight. Because of this unpredictability and also experimentation with relative beam intensities, many shots were fired before meaningful holographic results were obtained.

Among the first successful holograms were a series of single exposures taken while attempting to refine the timing of the laser pulse to coincide with projectile passage through the test area. Figure 12 is the reconstruction of one of these single exposure holograms containing a shadowgraph of the projectile. As an indication of the size of the projectile, the grid in the photograph is $\frac{1}{2} \times \frac{1}{2}$ centimeter. In this particular hologram, the detached bow shock wave is actually discernible. For easier viewing, the projectile and shock are redrawn in Figure 13.

The standoff distance of the shock at the nose of the projectile was 2.7 mm. The approximate nose radius of the projectile was 3.8 mm, yielding a standoff distance to nose diameter ratio of .355.

Van Dyke [Ref. 12] provides theoretical values of this ratio for a sphere as a function of Mach number. His values are obtained through an inverse method in which a marching technique is used to integrate numerically the flow equations from the shock to the sphere. Experimental measurements provided excellent agreement with these theoretical results.

A $\Delta s/d$ ratio of .355 indicated that the projectile Mach number was 2.2 in the region of elevated temperature just outside the muzzle. The precursor traveling shock, well ahead of the projectile at this point, is outside the view of this hologram.

The measured muzzle velocity for this particular shot was 3364 feet per second for a freestream Mach number of 3.0.

After resolving as well as possible the problem of timing the laser firing, double pulsed holography was conducted. Figure 14 is a finite fringe hologram of the precursor traveling shock emerging from the barrel ahead of the projectile. This shock was created by rapid expulsion of the gases within the barrel ahead of the projectile. At the point of exposure, this shock was 1.75 cm from the muzzle along the barrel axis and appears nearly spherical with a radius of 2.25 cm. The steep density gradients across the shock are evident by the extremely closely packed fringe pattern visible across the shock.

Figure 15 is another finite fringe hologram with the precursor traveling shock at a distance of 3.2 cm from the muzzle. At this point the shock radius had increased and had weakened appreciably as indicated by the wider spacing of the fringes. This hologram also reveals a second shock of smaller radius behind the first at 2.6 cm from the muzzle. This inner shock could have been a recompression wave due to overexpansion behind the outer shock wave. Further examination of this hologram also revealed the radial development of the Prandtl-Myer expansion fan around the rim of the muzzle face. The precursor shock from Figures 14 and 15 are redrawn together in Figure 16. As seen in this figure the limited size of the field makes fringe analysis difficult.

Figure 17 is a double-pulsed hologram taken with the nose of the projectile 2.4 cm into the field. The grid system is still in place and

its adverse effects are evident. In this figure a marker on the grid indicating the central portion of the test section is evident on the nose of the projectile.

Holograms of the projectile at increasing degrees of penetration of the flow field may be seen in Figures 18 through 21. Each of these holograms is a finite fringe hologram with varying degrees of fringe separation. The boundary layer was visible in Figures 18 and 21 in the sharp fringe shifts at the projectile surface. As the bullet progressed through the field, less of the field around the projectile was visible due to the limited view of the test area.

In Figure 21 nearly $2/3$ of the projectile had passed the center of the test section indicated by the vertical reference wire. With approximately one inch of projectile remaining, the field became blurred and the image of the bullet as well as the fringe pattern disappeared. The beginning of this process was also shown clearly in Figure 20. It is probable that the loss of image at this point was due to leakage of the high pressure combustion gases around the projectile. The flow of these gases is turbulent and tends to obscure the field. Additionally, the combustion effluents caused the gases to become opaque and difficult to observe holographically.

IX. COMPARISON OF ANALYTICAL AND EXPERIMENTAL RESULTS

Sample outputs from the computer program are illustrated in Figures 22 and 23. Figure 22 summarizes the major inputs including initial conditions in the approximate program output format. As seen in this figure, the time increment between printout of calculated flow parameters may be selected arbitrarily. The print interval for this particular run was .2 milliseconds. Figure 23 illustrates the output from the final cycle as the projectile leaves the barrel. The mass point, j , for the projectile is 6 and its velocity (muzzle velocity at this point) is 1064 meters per second. The X position is distance from the breech end to the mass point. Using printout from each cycle, the projectile velocity was plotted as a function of X-distance in Figure 24.

The mean experimental projectile velocity measured with the Oehler velocity screens over a series of 53 shots was 1032 meters per second for an average Mach number of 3.03. The velocities ranged from 1020 to 1056 meters per second and had a standard deviation of 10.7 meters per second. The measurement was taken at a distance of 2.68 meters from the muzzle. Assuming a projectile drag coefficient of .28 [Ref. 10], the average muzzle velocity was approximately 1033 meters per second. This measurement was within 3% of the predicted value.

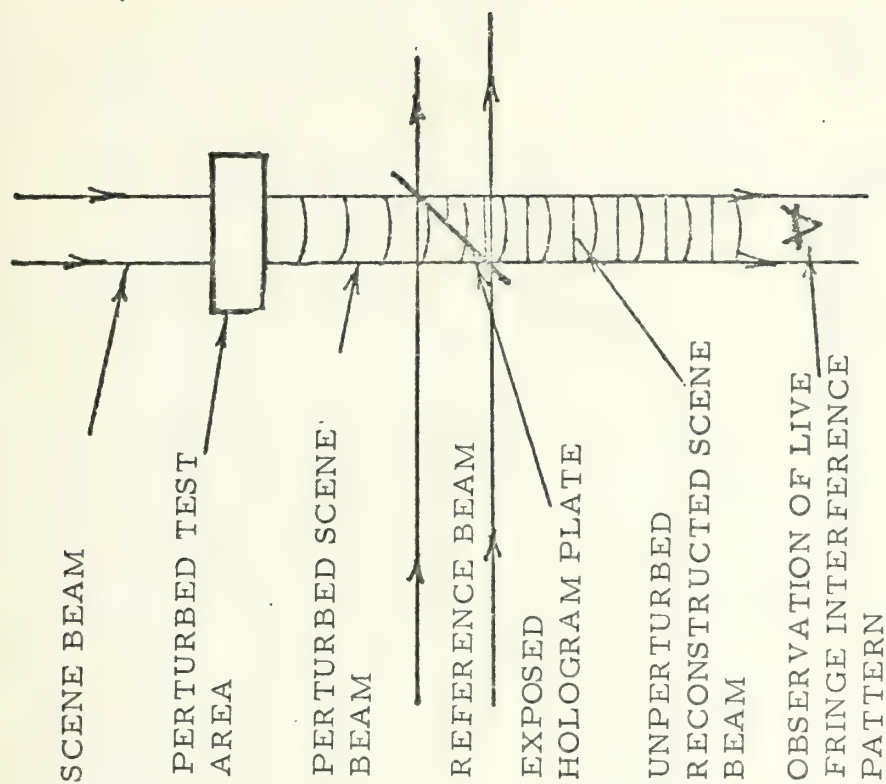
From Figure 23, the computed time of projectile arrival at the test section was 1884 microseconds after the firing pulse. Actual average time of arrival based on holographic evidence of the projectile in the test section was 1600 microseconds after triggering of the Kistler pressure transducer 14.0 centimeters from the breech end. This required a projectile travel of nearly 7 centimeters. From the computer program this estimated time of travel was 378 microseconds for a total of 1978 microseconds. Agreement between predicted and measured values is within 5%.

The computer pressure history at the transducer location was plotted using the zone pressure at the 14-centimeter location for each print cycle. This pressure trace is plotted in Figure 25 along with the actual measurements from the Kistler pressure transducer. Very good agreement was obtained between the actual and numerically obtained pressures. The experimental results show, after an initial overshoot, a peak pressure of 4966 bars at approximately .62 milliseconds after the firing pulse. The predicted pressure history rises and falls somewhat more rapidly than the actual trace, with a peak pressure of 5624 bars at .475 milliseconds after the firing pulse. Excellent agreement is seen between the actual and theoretical pressures after these initial peak values.

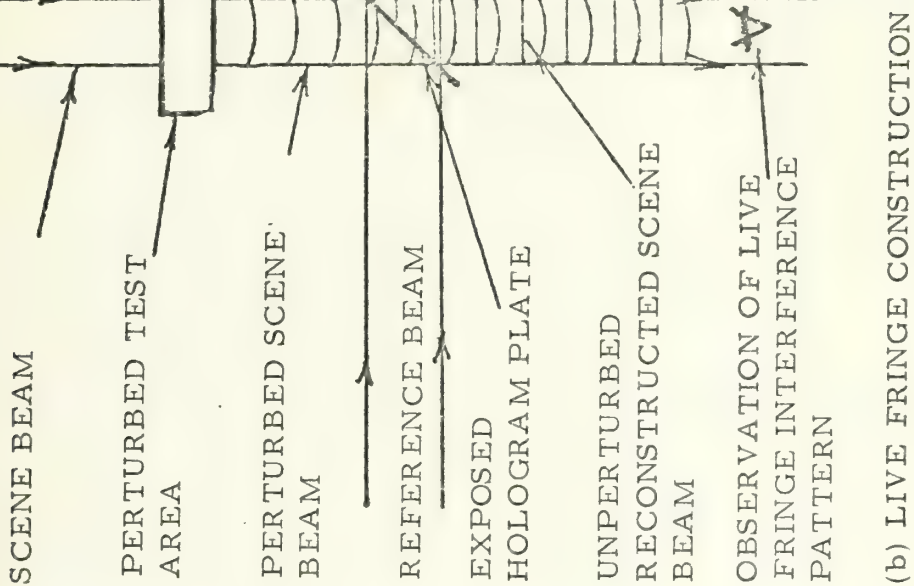
X. SUMMARY AND RECOMMENDATIONS

The numerical solution of the one-dimensional hydrodynamic equations has provided excellent agreement with experimentally measured flow parameters including muzzle velocity, pressure history, and projectile launch time. This program may be used in predicting these parameters under a wide range of initial conditions including variations in powder characteristics, and projectile and launcher size.

The feasibility of the use of holography in the visualization of exterior ballistic flow fields has been demonstrated. Several excellent holograms of the projectile and its associated flow field have been obtained. Interferometric analysis was restricted, however, due to the limited field of view obtained with the present optical arrangement which was initially designed to study interior ballistic flow fields. Currently, the optical arrangement is being modified to provide this enlarged field of view necessary for the interferometry. Additionally it is felt that imposition of a horizontal fringe field rather than the vertical field used in this study would be easier to analyze interferometrically because of the axi-symmetric nature of the flow field. This entails only vertical rather than horizontal rotation of the scene beam between exposures and requires no modification of the current optical arrangement.

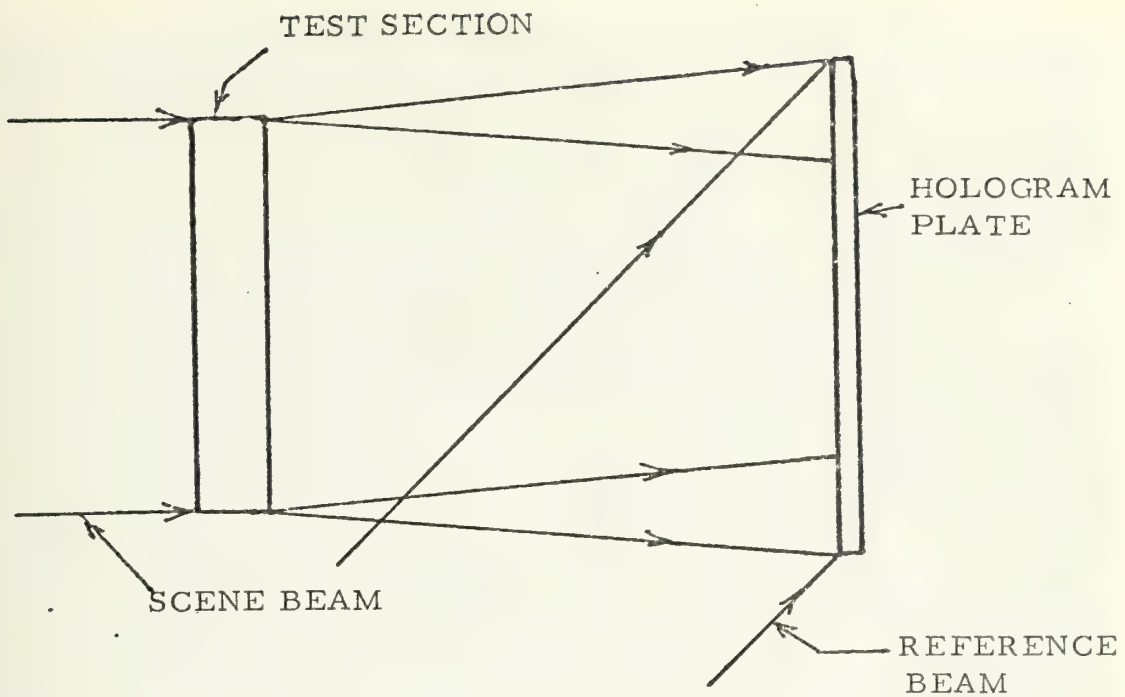


(a) EXPOSURE WITH UNPERTURBED SUBJECT BEAM

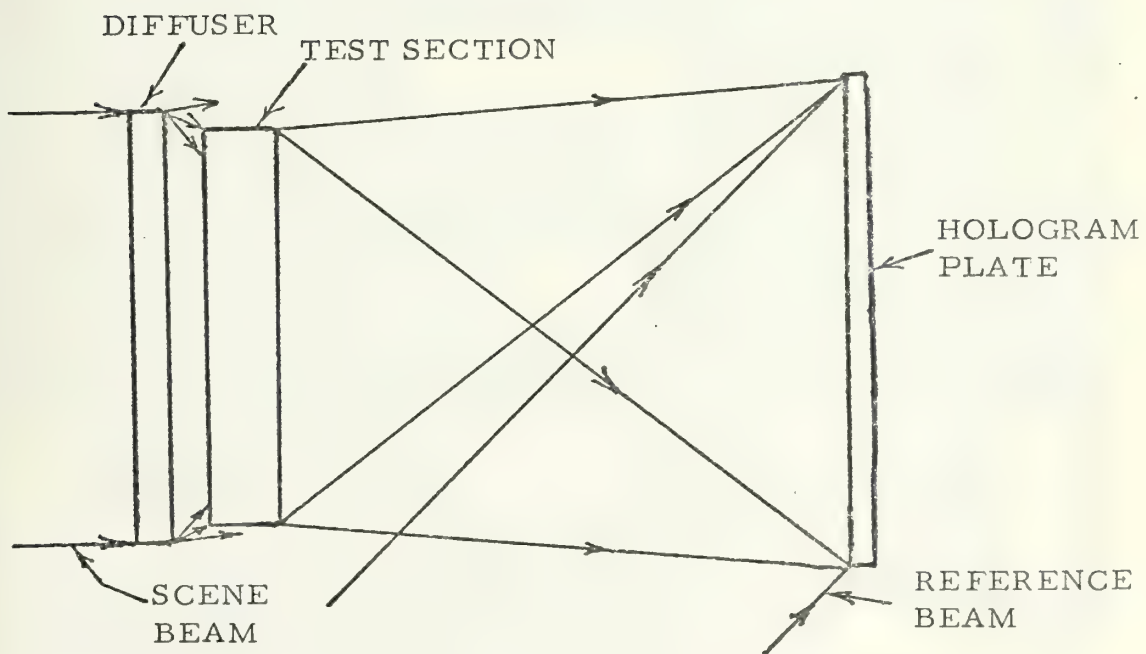


(b) LIVE FRINGE CONSTRUCTION

FIGURE 1.



(a) DIRECT ILLUMINATION



(b) DIFFUSE ILLUMINATION

FIGURE 2.

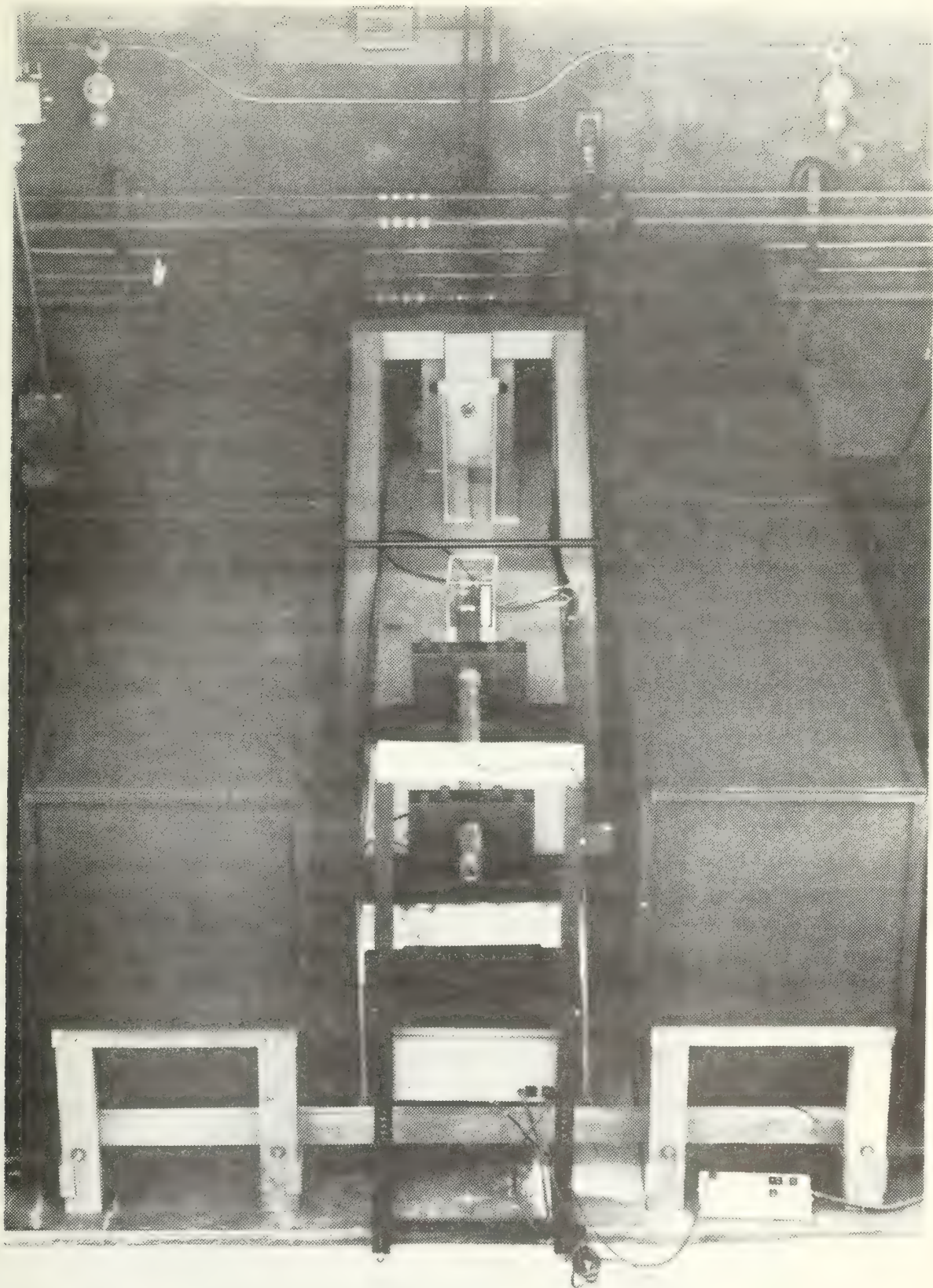


FIGURE 3. TEST CELL LAYOUT

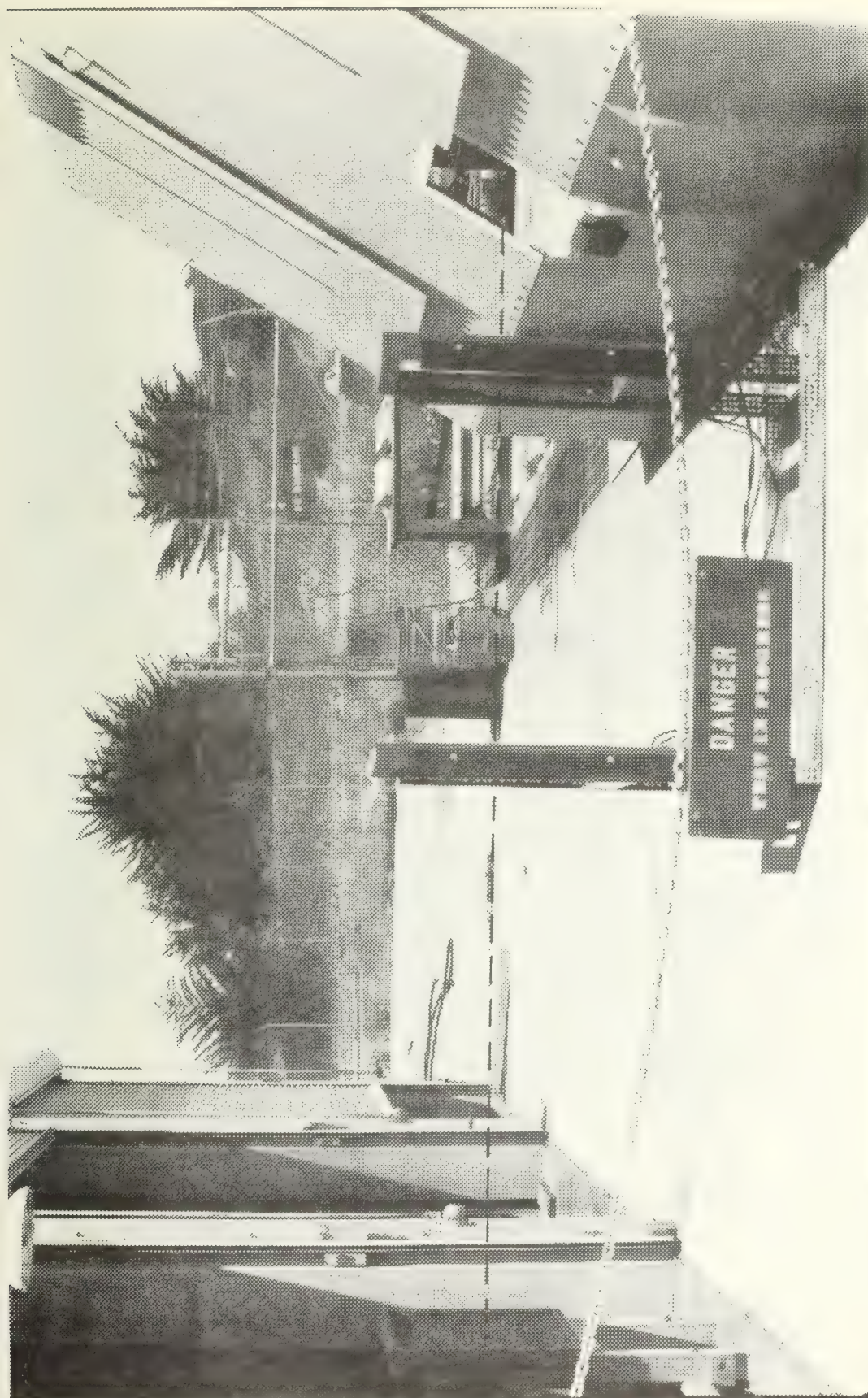


FIGURE 4. PROJECTILE PATH AND TURRET

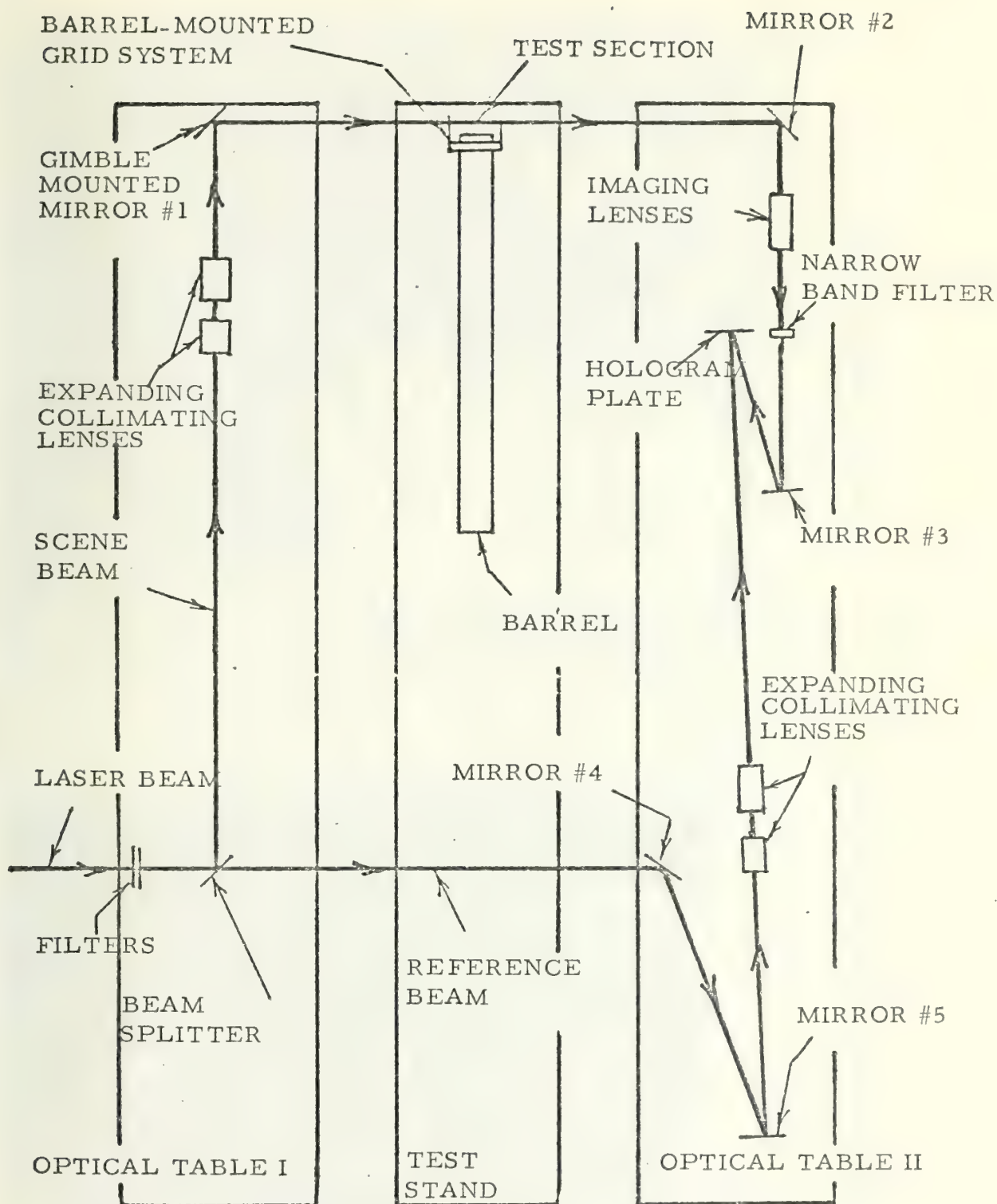
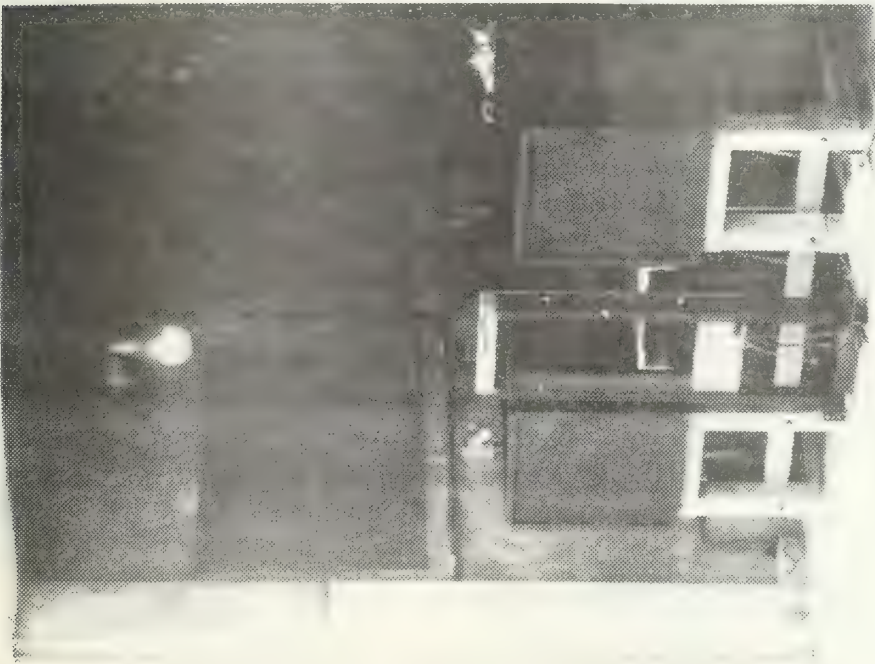
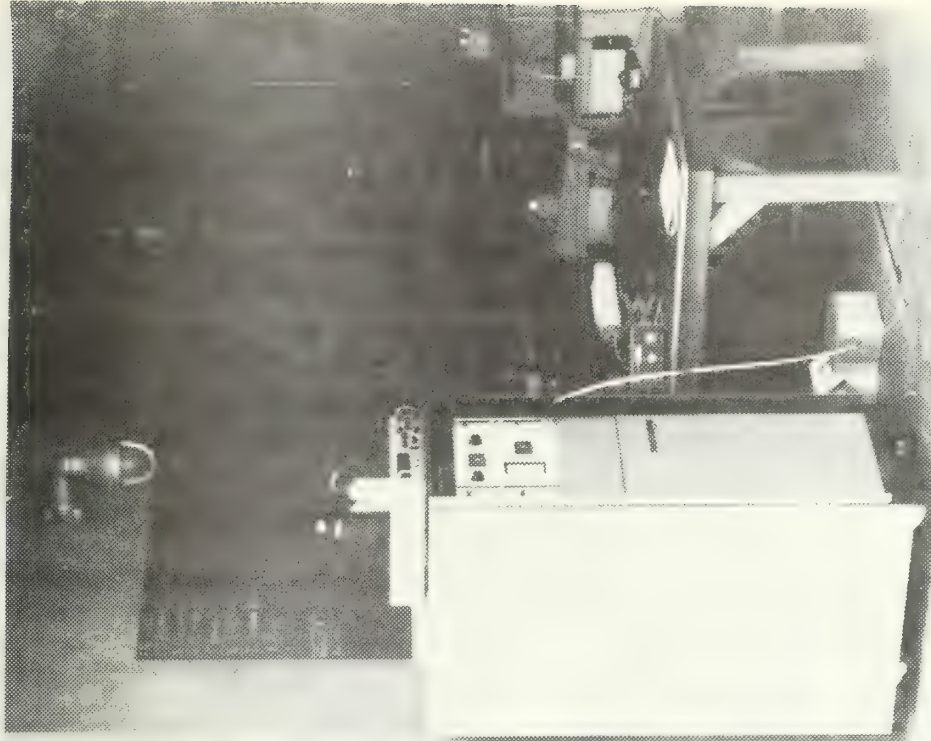


FIGURE 5. OPTICAL ARRANGEMENT



(b) CANNON AND OPTICS TEST CELL



(b) LASER INSTALLATION

FIGURE 6.



FIGURE 7. OPTICAL ARRANGEMENT

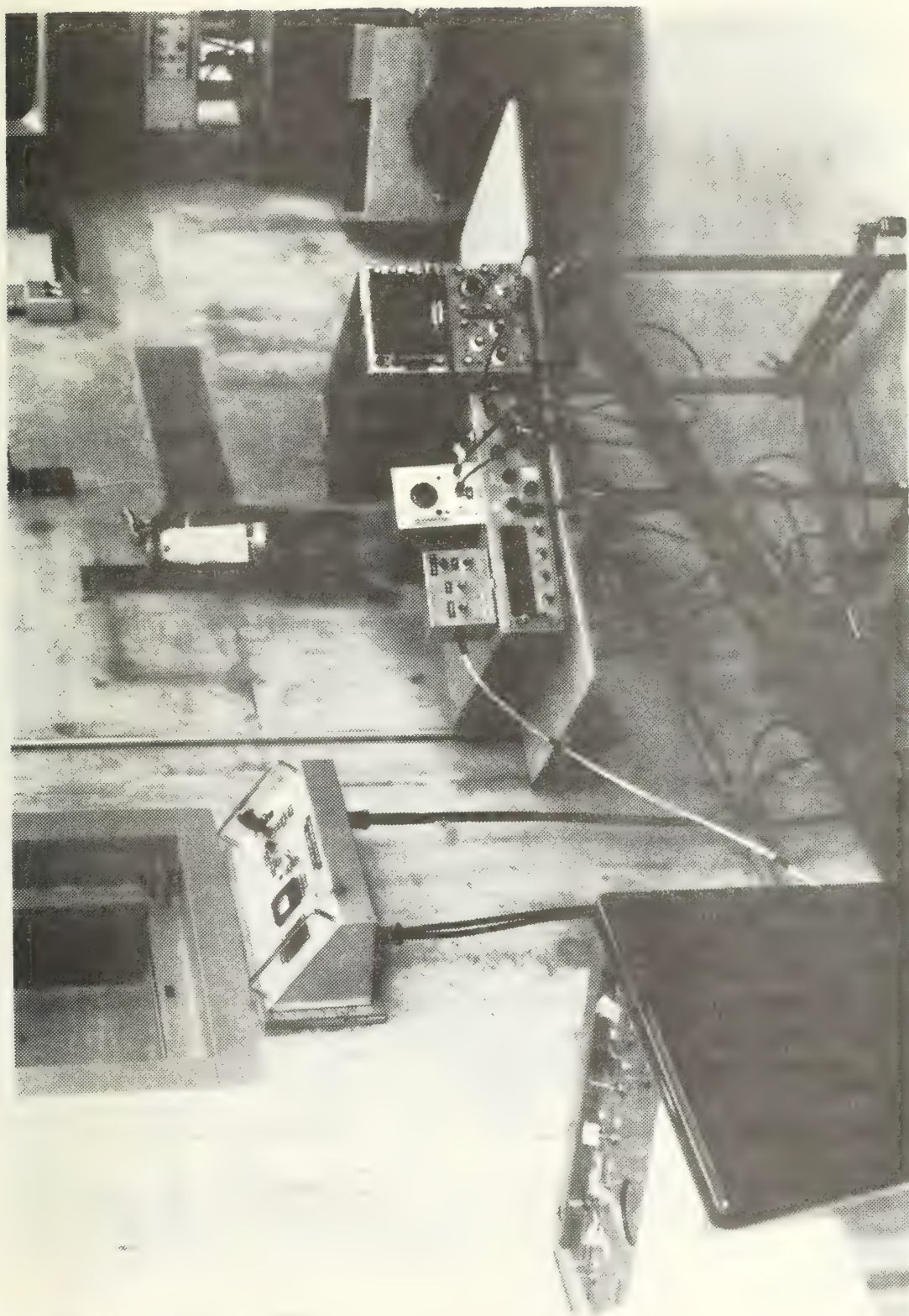


FIGURE 8. CONTROL ROOM INSTRUMENTATION

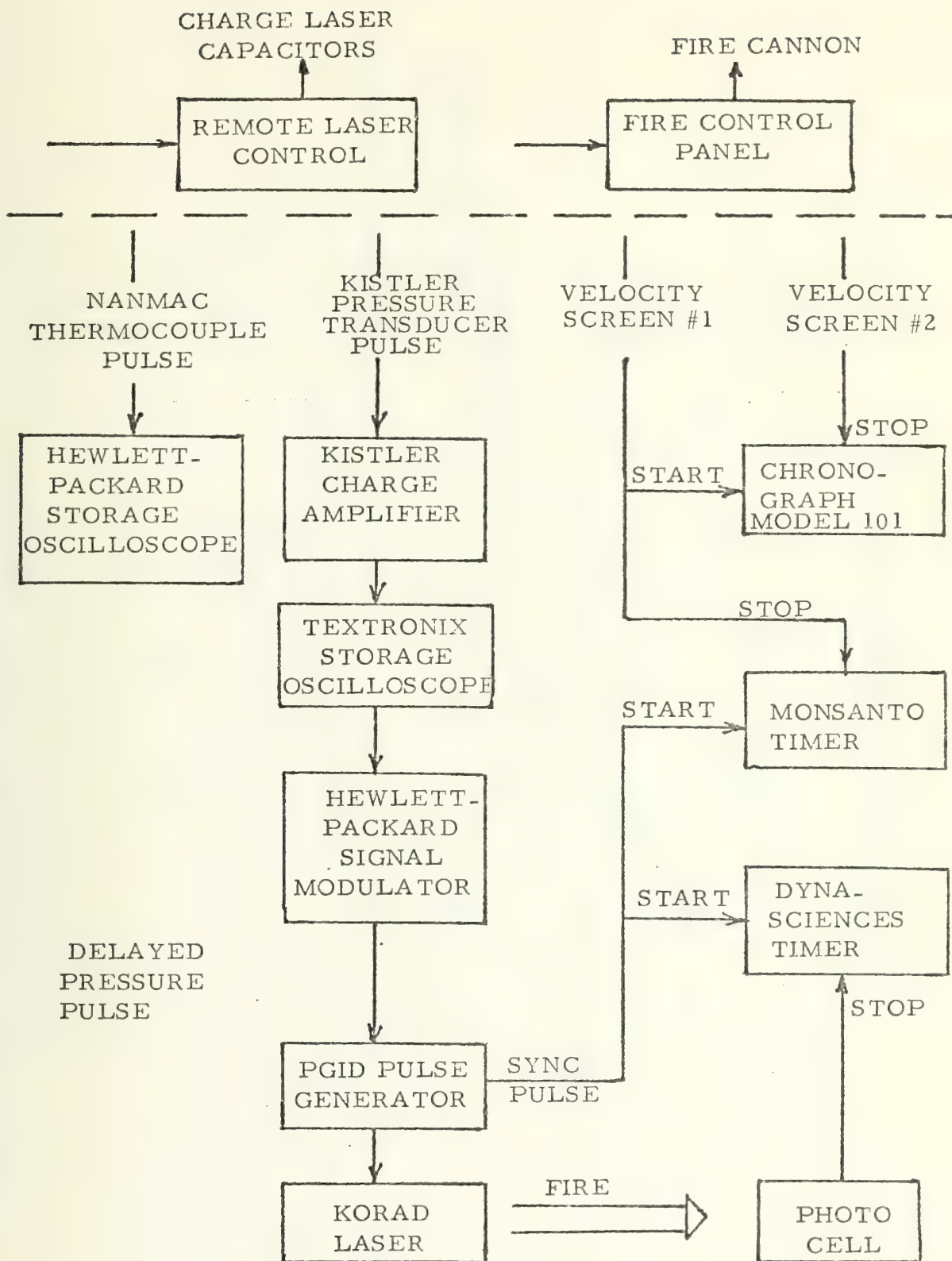


FIGURE 9. FIRING SEQUENCE

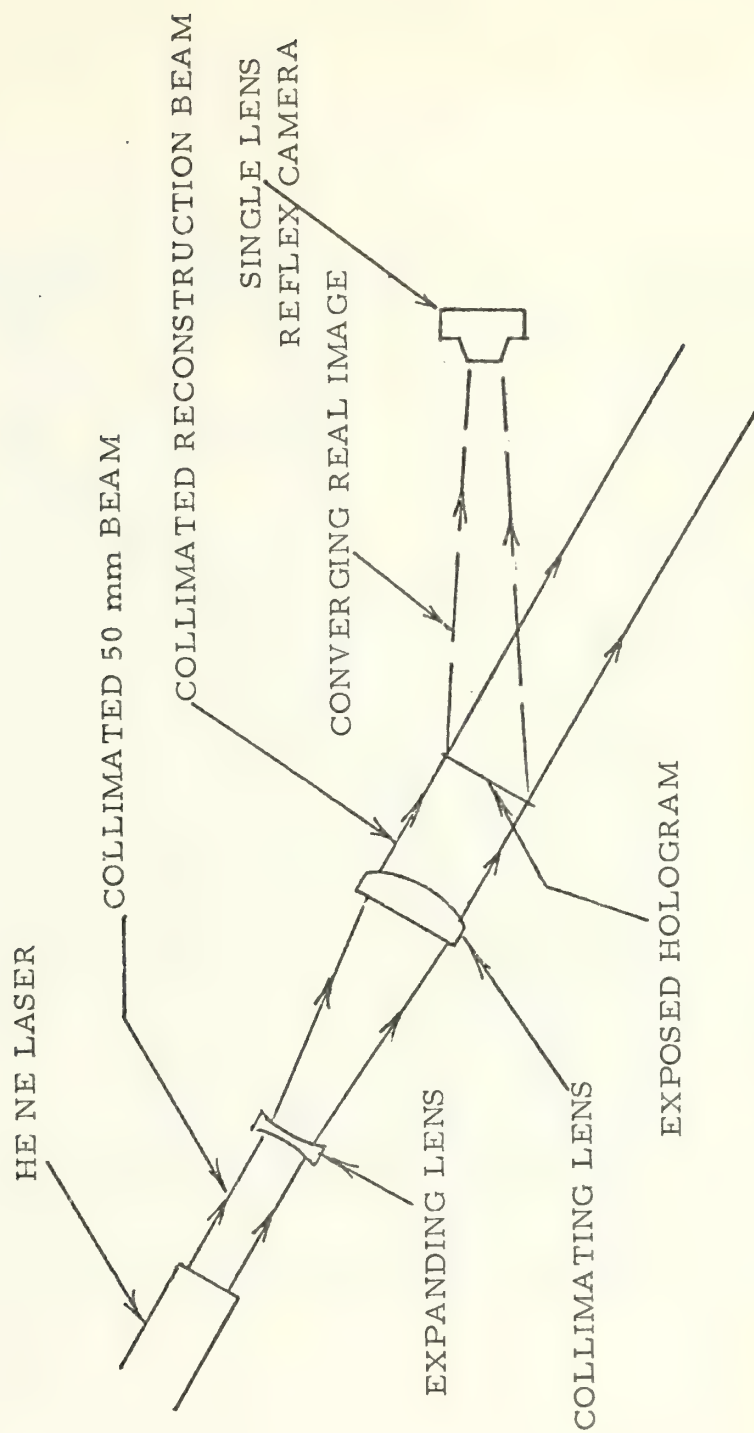


FIGURE 10. RECONSTRUCTION

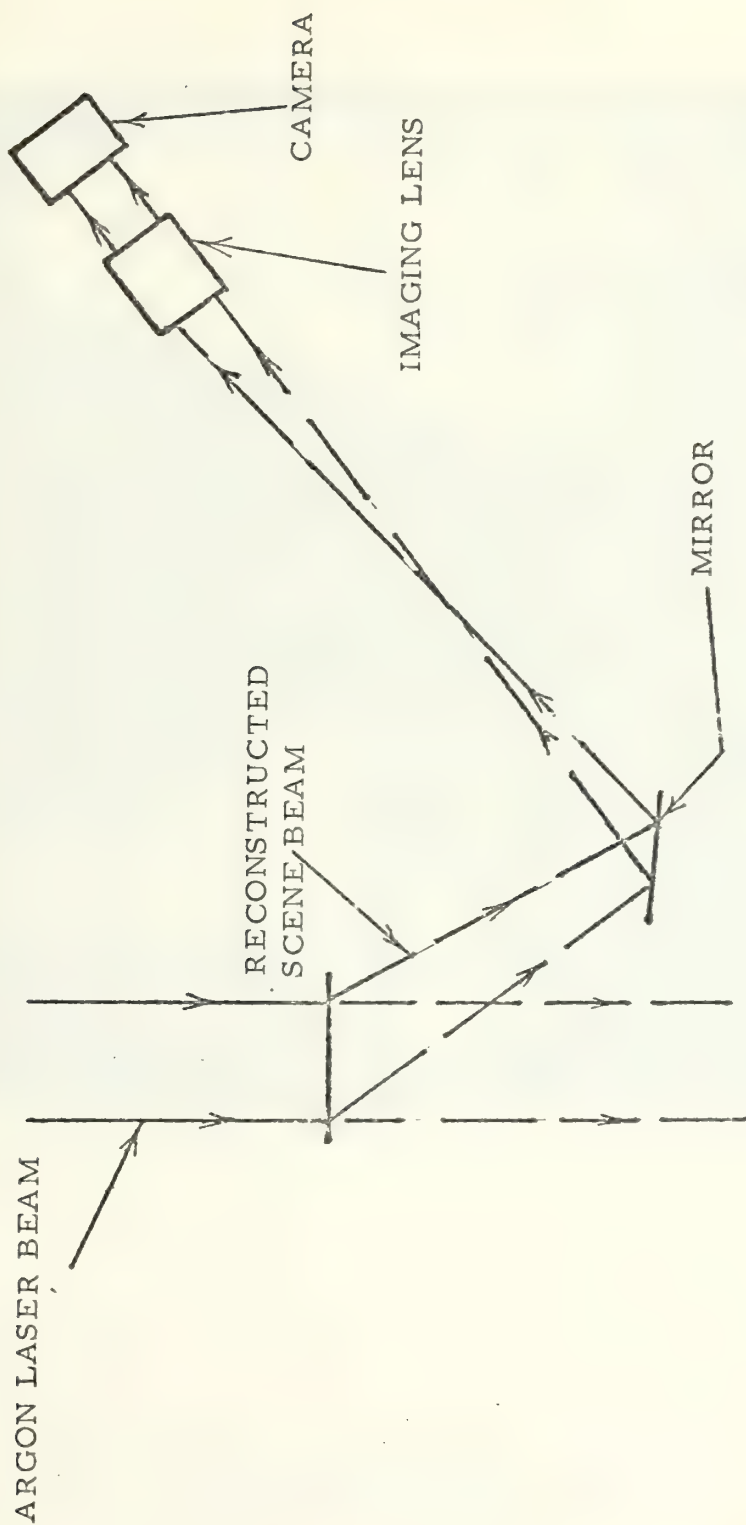


FIGURE 11. RECONSTRUCTION

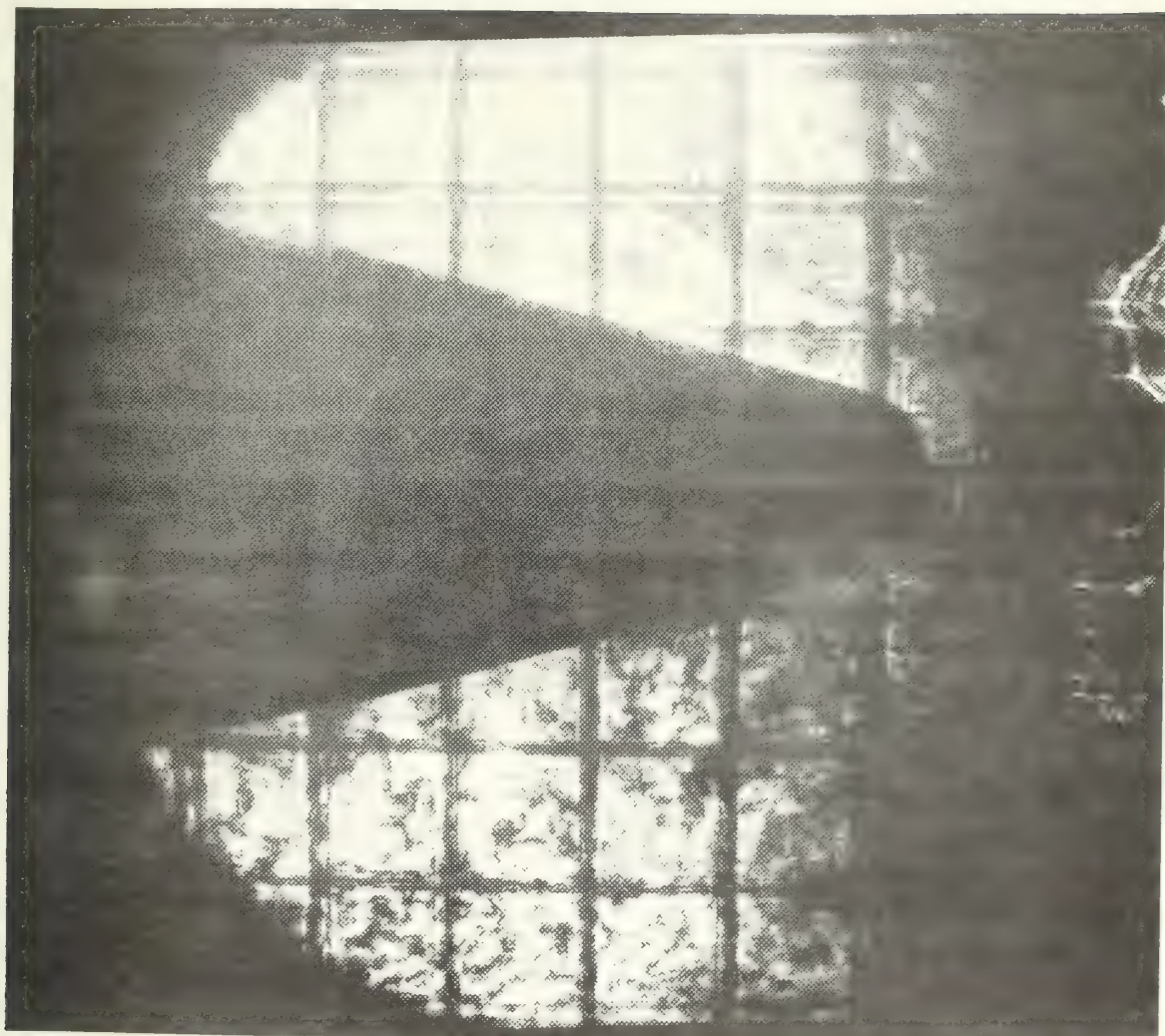


FIGURE 12. SINGLE EXPOSURE HOLOGRAM
OF PROJECTILE

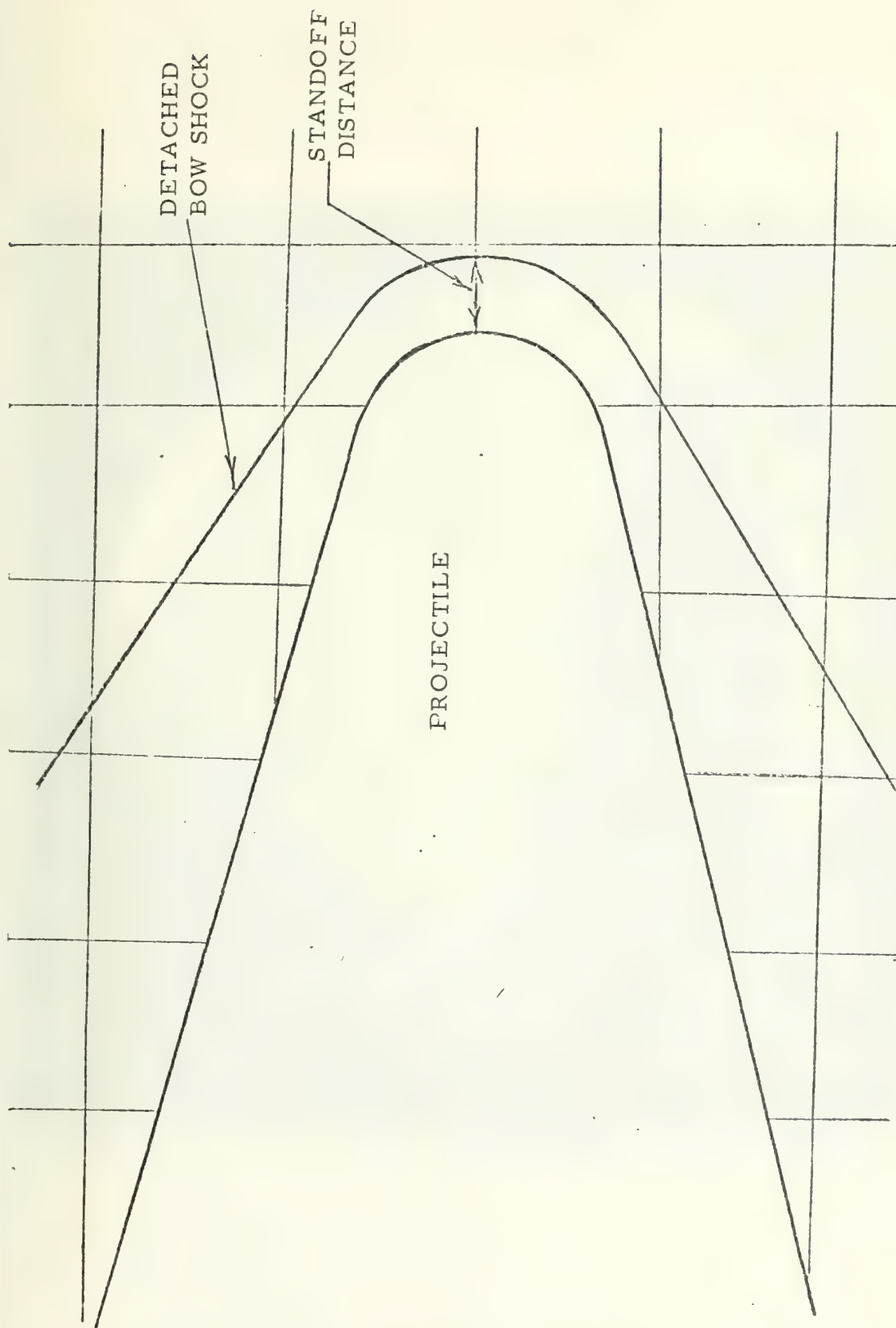


FIGURE 13. REDRAWN BOW SHOCK OF FIGURE 12

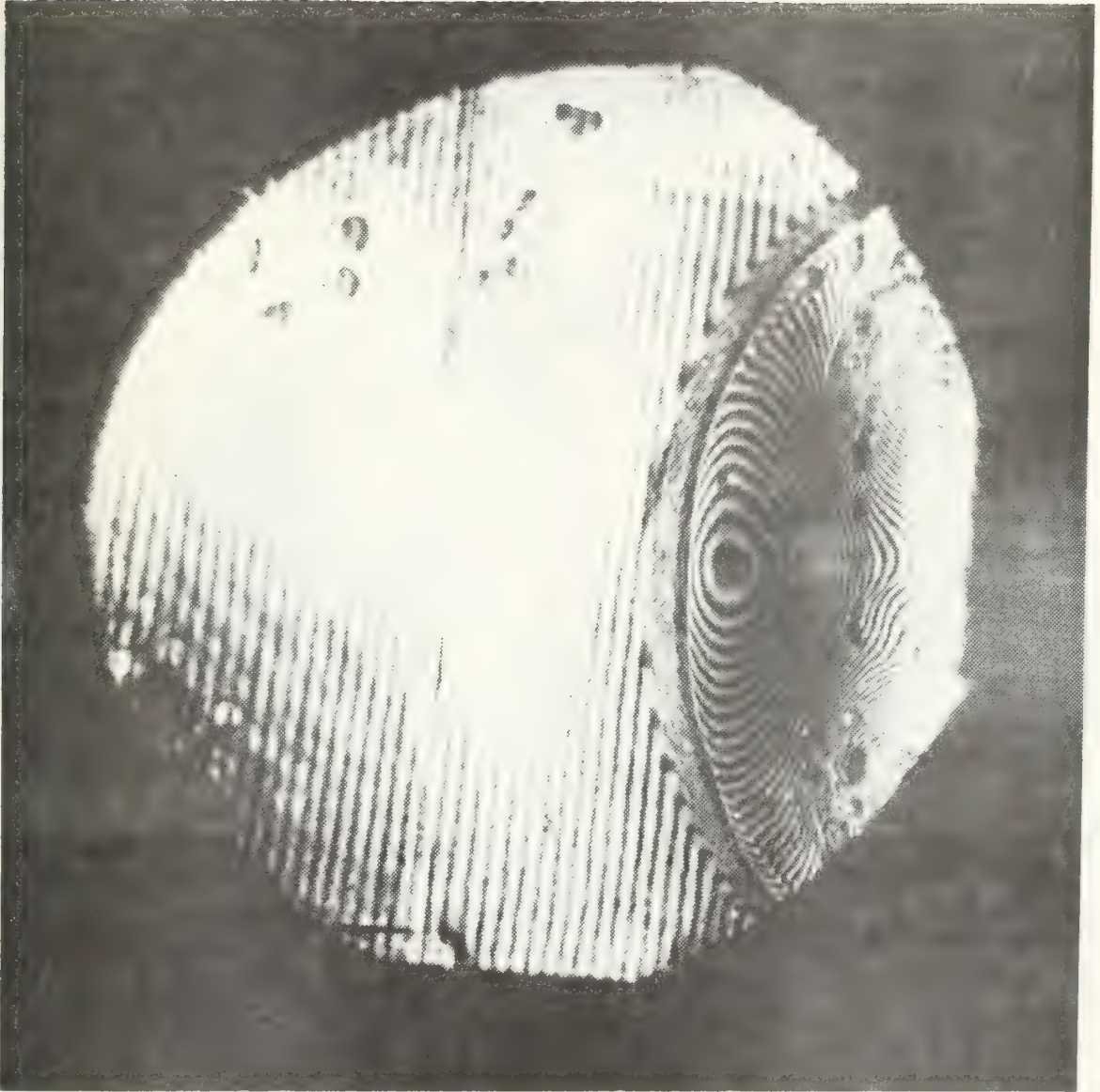


FIGURE 14. HOLOGRAPHIC INTERFEROGRAM OF
PRECURSOR TRAVELING SHOCK



FIGURE 15. HOLOGRAPHIC INTERFEROGRAM OF
PRECURSOR TRAVELING SHOCK

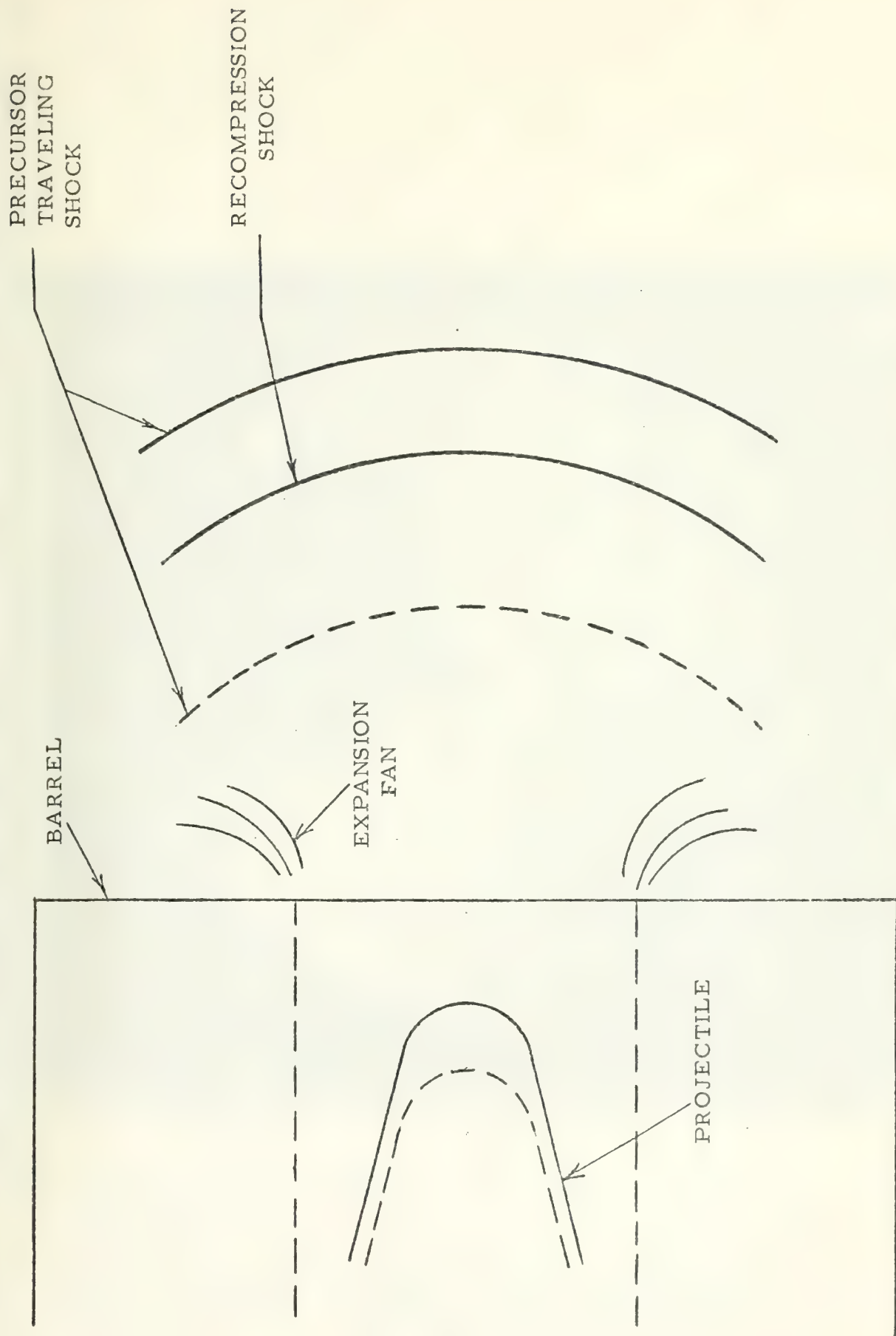


FIGURE 16. REDRAWN SHOCK SYSTEMS OF FIGURES 14 AND 15



FIGURE 17. DOUBLE PULSED HOLOGRAM
OF PROJECTILE



FIGURE 18. HOLOGRAPHIC INTER FEROGRAM
OF PROJECTILE

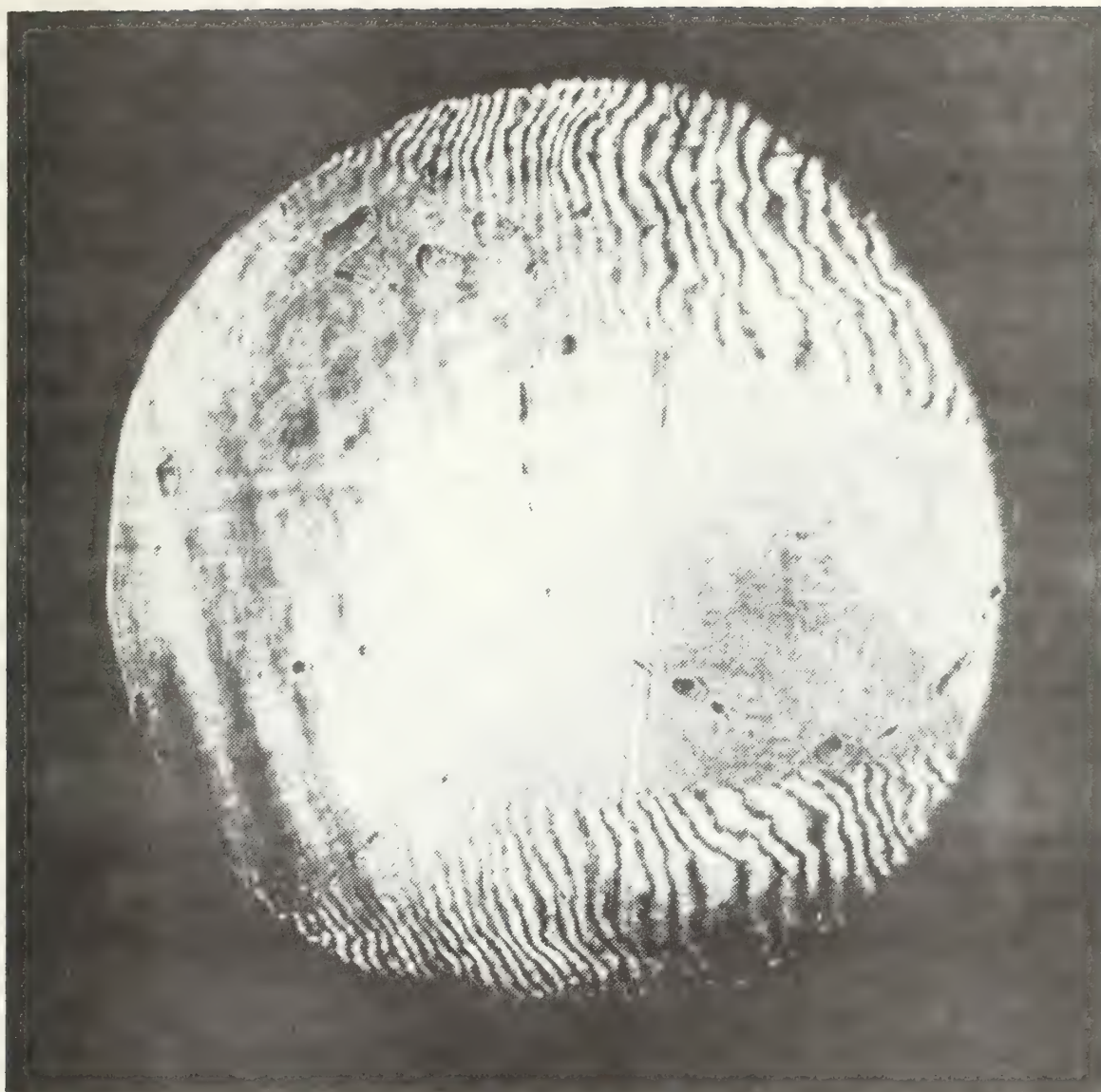


FIGURE 19. HOLOGRAPHIC INTERFEROGRAM
OF PROJECTILE



FIGURE 20. HOLOGRAPHIC INTERFEROGRAM
OF PROJECTILE

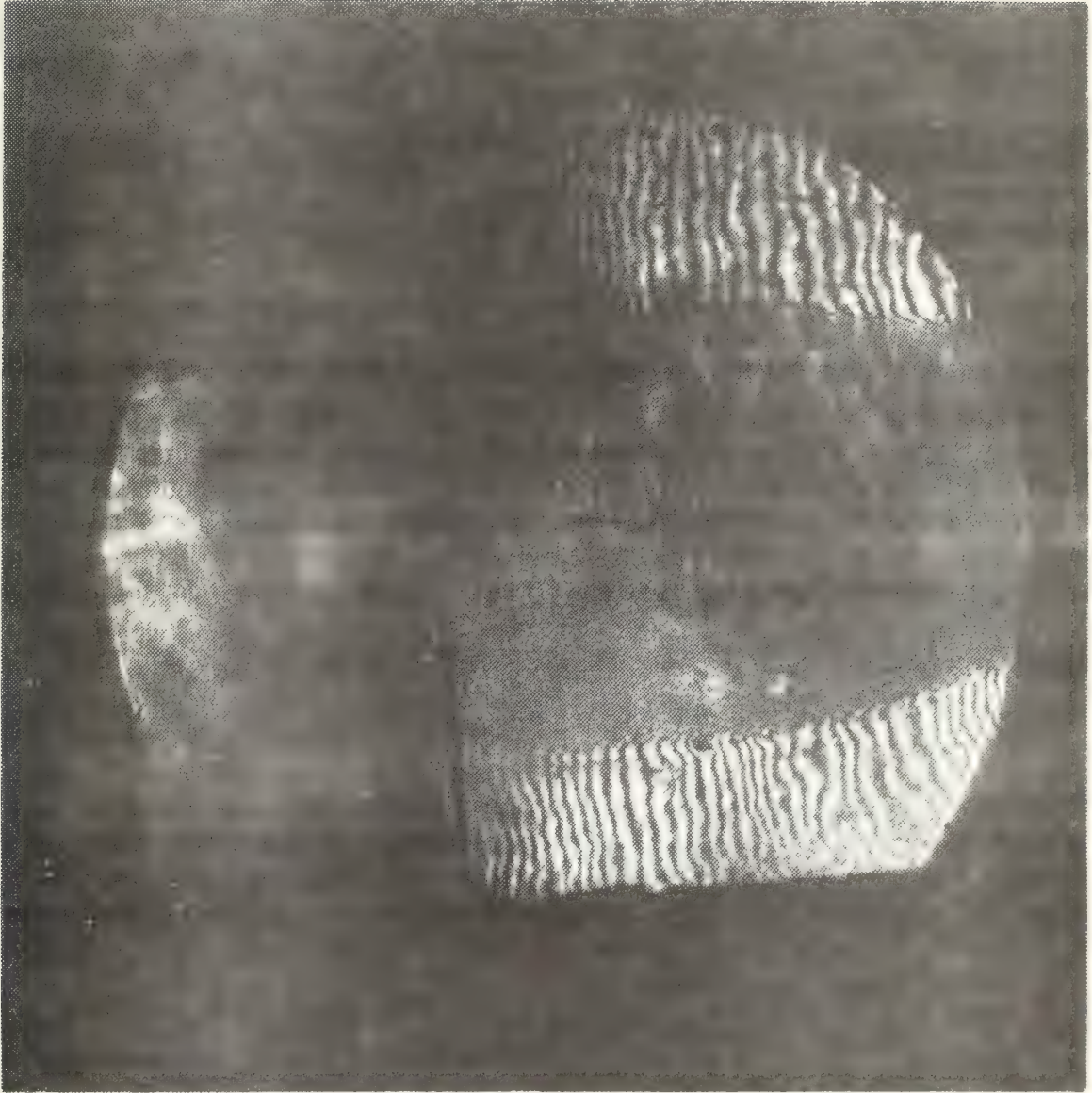


FIGURE 21. HOLOGRAPHIC INTERFEROGRAM
OF PROJECTILE

GUN BARREL PROJECT

Computer Run Number: 3

Date: 5/10/75

Dimensions: 6 Regions, 6 Zones

<u>Regions</u>	<u>Zones</u>	<u>Length (cm)</u>	<u>Area (cmsq)</u>	<u>Volume (cc)</u>
1	1	1.47	2.95	4.35
2	1	1.47	2.95	4.35
3	1	1.47	2.95	4.35
4	1	1.47	2.95	4.35
5	1	1.47	2.95	4.35
6	1	5.40	2.95	15.93

INITIAL CONDITIONS

Powder Conditions: Grams Powder = 38.23
TBURND = 1.000 Millisec

Materials:

<u>Region</u>	<u>NEQST</u>	<u>Pressure (psi)</u>	<u>Temp. (Deg. K)</u>	<u>Molec. Wt. (gm/mole)</u>
1	2	14.7	300.0	125.00
2	2	14.7	300.0	125.00
3	2	14.7	300.0	125.00
4	2	14.7	300.0	125.00
5	2	14.7	300.0	125.00
6	3		300.0	55.85

Print out every 0.20 millisec up to 10.00 millisec

Print out every 0.050 millisec up to break

Print out every 0.200 millisec up to launch

Mass of Projectile = 90.0 gm

Break Valve Strength = 690.0 Bars

Number of Pressure Points: 1

Location of Pressure Points: 14.0 cm

FIGURE 22. COMPUTER OUTPUT FORMAT

GUN BARREL PROJECT

Cycle 290	T(Millisec)	1.88443E 00	
	DT(Millisec)	2.18257E-02	

j	X (CM)	VELOCITY (CM/MS)	PRESSURE (BARS)
1	0.0	0.0	1.01381E 03
2	1.46490E 02	1.01004E 02	8.52849E 02
3	1.47602E 02	1.03653E 02	7.78181E 02
4	1.48734E 02	1.06449E 02	8.85098E 02
5	1.49668E 02	1.07232E 02	1.05442E 03
6	1.50551E 02	1.06399E 02	3.98267E 02

FIGURE 23. COMPUTER OUTPUT FORMAT



FIGURE 24. PROJECTILE VELOCITY vs. POSITION

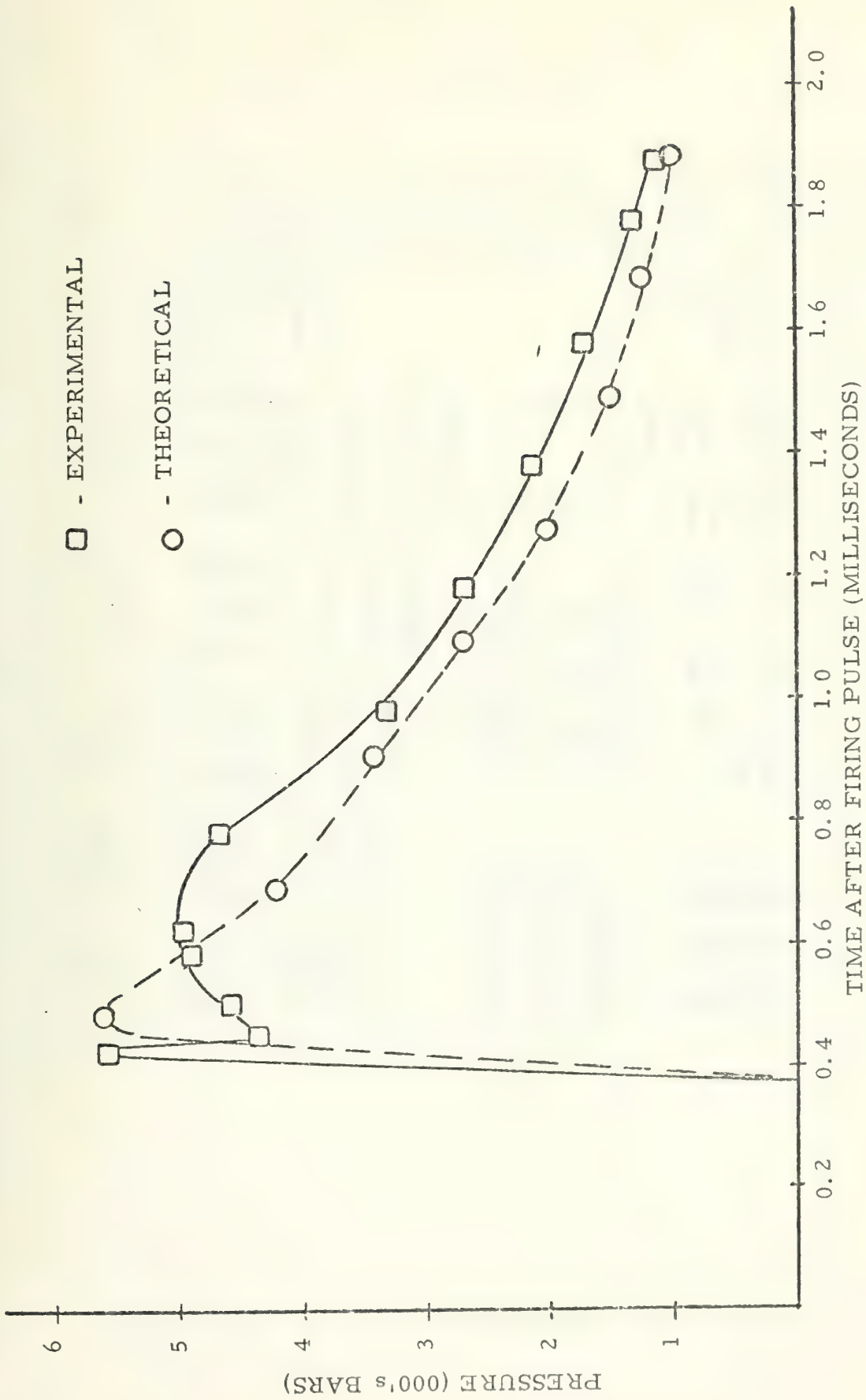


FIGURE 25. PRESSURE (14 cm FROM BREECH) vs. TIME

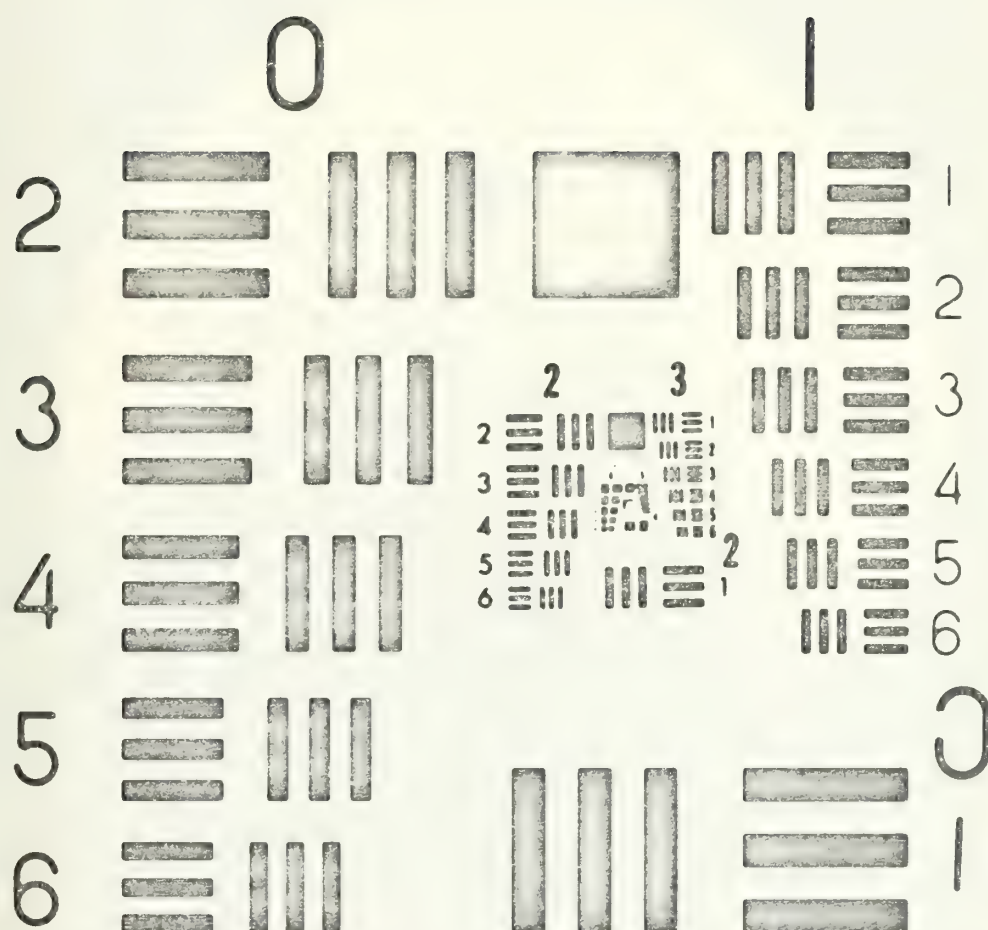


FIGURE 26. USAF 1951 RESOLUTION TEST TARGET



FIGURE 27. HOLOGRAM OF USAF 1951 RESOLUTION
TEST TARGET

2

U

65


```

123 NI = 0
M = 6
NPVITR = 1
1 CALL ZECAB(500,XP1,XP2,PP1,VP2,XP3)
CALL ZEROA(500,PP3,PP1,PP1,PP1)
CALL ZEROA(10,ISTOPX,ISTOPX,ISTOPX,ISTOPX)
INTERJ(31)=M
CPMAX=0.0
PTMAX=0.0
AMPNAX=0.0
NTIMPT=0
IP=0
NPUNCH=1
IPNCH=0
LN = 0
IPV1 = 1
IPV2 = 2
HYDRD1=13.3
HYDRD2=1
END INITIAL CONDITIONS FOR PROGRAM, BEGIN INPUT FOR RUN, NEW OR ITE
IF (NPVITR.EQ.1) GO TO 41
NPVITR = 1
INPUT FOR STORAGE
CALL STORE(ISTORM, STORM)
EMLEAD=STORM(97)
HYDRD1 = STORM(98)
HYDRD2 = STORM(99)
NEQST(30) = ISTORM (100)
IF (IDATA) 8,8,608
41 CONTINUE NEW RUN, STORAGE OF INPUT
READ(5,604)IDATA,I PRNTZ,ITRNSF,IPUNCH,DTSQ(199)
FORMAT(413,F10.0)
604 IF (ITRNSF.EQ.0) GO TO 619
M = 6
INTERJ(31)=M
619 IF (IDATA) 606,606,620
608 READ(5,READ1)
ICATA=0
GO TO 610
606 CALL READ
READ(5,20) IPOX, NPOX, (XPO(K), K=1, NPOX)
READ(5,49) XPV1, XPV2, PVER, PVWANT
READ(5,6)P,EMPIS,FRAC,EMLEAD
FORMAT(E10.4,3F10.0)
6 READ(5,49) (PO(I),I=1,IMAX)
READ(5,49) (TO(I),I=1,IMAX)

```

HVMN 0390
HVMN 0400
HVMN 0410
HVMN 0420
HVMN 0430
HVMN 0440
HVMN 0450
HVMN 0460
HVMN 0470
HVMN 0480
HVMN 0490
HVMN 0500
HVMN 0510
HVMN 0520
HVMN 0530
HVMN 0540
HVMN 0550
HVMN 0560
HVMN 0565
HVMN 0566
HVMN 0570
HVMN 0580
HVMN 0590
HVMN 0600
HVMN 0610
HVMN 0620
HVMN 0630
HVMN 0640
HVMN 0650
HVMN 0660
HVMN 0670
HVMN 0680
HVMN 0690
HVMN 0700
HVMN 0710
HVMN 0720
HVMN 0730
HVMN 0740
HVMN 0750
HVMN 0760
HVMN 0770
HVMN 0780
HVMN 0790
HVMN 0800
HVMN 0810
HVMN 0820
HVMN 0830
HVMN 0840


```

      READ (5,49) (AMOL(I), I=1, IMAX)
      FORMAT(7F10.0)
      CONTINUE
      CALL STORIN (ISTORM, STORM)
      STORM(97)=EMLEAD
      STORM(98)=HYDRD1
      STORM(99)=HYDRD2
      ISTJRM(100)=IPOX
      INITIAL CONDITIONS AND CONSTANTS FOR RUN
      8 INPTN=NZONES(1)+NZONES(2)+NZONES(3)+1
      N:XSST=FRAC*OUTBDY(5)
      NEQST(30)=IPCX
      CALL CALCUL (EMLEAD)
      IF(N1.NE.0)GO TO 603
      CALL PRNTC(EMLEAD,FRAC,XPV1,XPV2,PVWANT,NPOX,IPOX,XPO)
      IF(I1.PRNTZ.EQ.0)GO TO 603
      READ(5,11)ILASTK
      IF(ILASTK)123,12,1
      CALL SETUP
      DO 706 IMP=1, JLAST
      PMDMIN(IMP)=PPLUSQ(IMP)
      PMDMAX(IMP)=PPLUSQ(IMP)
      706 MAIN LOOP OF PROGRAM - DYNMEQ, LFTOVER, AND OUTPUT
      2 CALL DYNMEQ
      CALL LFTOVR(IPNCHX)
      DO 710 IMP=1, JLAST
      IF(PPLUSQ(IMP).GT.PMDMIN(IMP)) GO TO 705
      PMDMIN(IMP)=PPLUSQ(IMP)
      TMDMIN(IMP)=T
      705 IF(PPLUSQ(IMP).LT.PMDMAX(IMP)) GO TO 710
      PMDMAX(IMP)=PPLUSQ(IMP)
      TMDMAX(IMP)=T
      710 CONTINUE
      H.EQ.0.OR.JPROJ.NE.300) GO TO 627
      IF(TPUNCH.NPUNCH)=T-DTSQ(200)
      PRSTAB(NPUNCH+1
      NPNP1=TPUNCH+1
      JPLHAF=INTERJ(6)
      J=JPLHAF
      JMNHAF=JPLHAF-1
      DUD1=26./18.*PPLUSQ(JMNHAF)-1./9.*PPLUSQ(JMNHAF-1)
      PRSTAB(NPNP1)=DUD1
      707 IF(T.GT.(DTSQ(200)+DTSQ(199))) GO TO 647
      PRSTAB(NPNP1)=PRSTAB(NPNP1)*{(T-DTSQ(200))/DTSQ(199)}
      647 NPUNCH=NPUNCH+25,625,627
      IF(91-NPUNCH)625,625,627
      PUNCH 641, PRSTAB
      625 PUNCH 641, PRSTAB
      641 FORMAT(3(F12.8,E12.8))
      NPUNCH=1

```

HVMN 0850
 HVMN 0860
 HVMN 0870
 HVMN 0880
 HVMN 0890
 HVMN 0900
 HVMN 0910
 HVMN 0920
 HVMN 0930
 HVMN 0940
 HVMN 0950
 HVMN 0960
 HVMN 1110
 HVMN 1120
 HVMN 1130
 HVMN 1140
 HVMN 1150
 HVMN 1160
 HVMN 1170
 HVMN 1180
 HVMN 1190
 HVMN 1200
 HVMN 1210
 HVMN 1220
 HVMN 1230
 HVMN 1240
 HVMN 1250
 HVMN 1260
 HVMN 1270
 HVMN 1280
 HVMN 1290
 HVMN 1300
 HVMN 1310
 HVMN 1320
 HVMN 1330
 HVMN 1340
 HVMN 1350
 HVMN 1360
 HVMN 1370
 HVMN 1380
 HVMN 1390
 HVMN 1400
 HVMN 1410
 HVMN 1420
 HVMN 1430
 HVMN 1440
 HVMN 1450
 HVMN 1460

C	52	PROGRAM TO FIND MAX IN REGION TO GO HERE	HVMN2340
C	7	CONTINUE	HVMN2350
	5	STORAGE OF MODEL PLOTS AFTER BREAK VALVE	HVMN2360
	10	IF(JPROCJ-300) 13,5,13	HVMN2370
	13	IF(IP.GT.498) GO TO 2	HVMN2380
	9	IP=IP+1	HVMN2390
	35	IF(XSTOP.EQ.3000.) GO TO 76	HVMN2400
	36	XP1(IP)=X(JLAST,N)	HVMN2410
	80	XP2(IP)=X(JLAST,N)	HVMN2420
	70	PP1(IP)=PPLUSQ(INER51)	HVMN2430
	76	VP2(IP)=U(JLAST,NMNHAF)	HVMN2440
	93	GO TO 2	HVMN2450
	25	POINT OF RETURN TO MAIN LOOP OF PROGRAM	HVMN2460
	26	FINAL STORAGE OF POINTS TO BE PLOTTED, AND WRITING OF ALL PLOT TAP	HVMN2470
	27	IF(IPCX.EQ.5) GO TO 25	HVMN2480
	28	IF(IPCX.EQ.6) GO TO 76	HVMN2490
	29	IP=IP+1	HVMN2500
	30	XP1(IP)=X(JLAST,N)	HVMN2510
	31	XP2(IP)=X(JLAST,N)	HVMN2520
	32	PP1(IP)=PPLUSQ(INER51)	HVMN2530
	33	VP2(IP)=U(JLAST,NMNHAF)	HVMN2540
	34	GO TO 36	HVMN2550
	35	NPOX=1	HVMN2560
	36	IPLTX=1,NPOX	HVMN2570
	80	NP1TX=NP1PL(IPLTX)	HVMN2580
	70	IF(NP1TX.LT.10) GO TO 70	HVMN2590
	76	NP1TX=NP1PL(IPLTX)	HVMN2600
	93	DO 80 ITPP=1,NP1TX	HVMN2610
	25	IPLT(IITPP)=TPOX(ITPP)	HVMN2620
	26	PPLT(IITPP)=DUMVAR(IITPP, IPLTX)	HVMN2630
	27	IF(JPROCJ.NE.300) GO TO 1	HVMN2640
	28	CCNT=0	HVMN2650
	29	GO TO 25	HVMN2660
	30	DO 93 ITPP=1, LN	HVMN2670
	31	PPLT(IITPP)=DUMVAR(IITPP,1)	HVMN2680
	32	CONTINUE	HVMN2690
	33	TERMINATION OF RUN, RETURN FOR NEW INPUT	HVMN2700
	34	READ(5,1) ILATK	HVMN2710
	35	IF((IPUNCH.EQ.0).OR.(NPUNCH.EQ.1)) GO TO 629	HVMN2720
	36	NPUNCH=NPUNCH+1	HVMN2730
	37	PUNCH 641, (PRSTAB(IPXX), IPXX=1,NPUNCH)	HVMN2740
	38	CONTINUE	HVMN2750
	39	WRITE(6,45) CPMAX, PTMAX, AMPMAX	HVMN2760
	40	WRITE(6,704) ((IT,PMDMIN(IT),TMDMAX(IT),TMDMAX(IT)),	HVMN2770
	41	IT=1,JLAST)	HVMN2780
	42	FORMAT(13,2X,E12.6,2X,E12.6,2X,E12.6)	HVMN2790
	43	FORMAT(3F20.2)	HVMN2800
	44	IF(ILATK) 15, 12, 1	HVMN2810
	45		HVMN2820
	629		HVMN2830
	704		HVMN2840
	705		HVMN2850
	706		HVMN2860
	707		HVMN2870
	708		HVMN2880
	709		HVMN2890
	710		HVMN2900
	711		HVMN2910
	712		HVMN2920


```

15 WRITE(6,44)(NI,((A VEL(I),ALOAD(I),AGAS(I)),I=1,NI))
GO TO 123
12 STOP
20 FORMAT (2I2,7F10.0)
44 FORMAT (I3/(3F10.0))
11 FORMAT (I3)
11 END

```

```

HVMN 2930
HVMN 2940
HVMN 2950
HVMN 2960
HVMN 2970
HVMN 2980
HVMN 2990

```


.....

```

WRITE(6,111) CALPGM,TBURN,D,GMSPPDR,GASPRS
WRITE(6,106) (I,NEQST(I),PO(I),TO(I),AMOL(I),CQSQX4(I),I=1,IMAX)
WRITE(6,108) (I,GAMMA(I),EZERO(I),ROZERO(I),VZERO(I),I=1,IMAX)
WRITE(6,109) R
WRITE(6,110) XPV1,XPV2,PVWANT
WRITE(6,114) OUTDT1,TMAX1,OUTDT2,TMAX2
WRITE(6,115) EMLEAD*453.59
EMLEAX=EMPIST*453.59
EMPISX=EMPIST*453.59
XXMAS=REGVCL(IMAX)*ROZERO(IMAX)
SHPPRX=SHPR*14.504
WRITE(6,112) EMLEAD,EMLEAX,EMPIST,EMPISX,XXMAS
WRITE(6,113) SHPR,SHPRX
KQX=IPOX+1
GO TO(10,11,12,12,12,13,14),KQX
10 WRITE(6,119) IPOX
11 WRITE(6,120) IPOX
12 WRITE(6,123) IPOX
13 WRITE(6,121) IPOX
14 WRITE(6,122) IPOX
15 WRITE(6,116) NPOX
WRITE(6,117) (XPC(I),I=1,NPOX)
WRITE(6,118) FRAC
WRITE(6,65)
RETURN
100 FORMAT(23X,36HHYPERVERLOCITY MODEL LAUNCHER PROGRAM//22X,19HCOMPUTE
1P RUN NUMBER,15,7H DATE,12,1H/,12,1H/,12)
102 FORMAT(1H/34X,14HGUN DIMENSIONS/31X,12,10H REGIONS,13,6H ZONES
1//12X,6HREGION,5X,5HZONES,6X,6HLENGTH,9X,4HAREA,11X,6HVOLUME/35X,4
2H(CM)),9X,6H(CMSQ),11X,4H(CC)/1H)
103 FORMAT(14X,12,9X,12,2X,F10.2,5X,F10.2,7X,F10.2)
104 FORMAT(14X,12,9X,12,2X,F10.2,11X,3H---,12X,3H---)
105 FORMAT(1H/19X,7HSLOPE=,F8.4,9X,7HANGLE=,F6.2,5H DEG)
106 FORMAT(1H/5X,12HMATERIALS ---//7X,6HREGION,5X,5HNEQST,5X,8HPRESSUR
1E,7X,4HTEMP,9X,12,8X,F7.2,6X,F9.4,6X,F5.1)
29H(GM/MOLE)/1H)
108 FORMAT(9X,12,8X,12,5X,F9.2,6X,F7.2,6X,F9.4,6X,F5.1)
109 FORMAT(1H/6X,6HREGION,4X,5HGAMMA,9X,6HNEPGY,10X,7HDENSITY,9X,9HS
1P VOLUME/26X,13H(BARS-CC/CC),7X,7H(GM/CC),9X,8H(CC/CC)/1H)
110 FORMAT(8X,12,5X,18HINITIAL CONDITIONS/5X,20HPOWDER CONDITIONS ---//
111 FORMAT(1H//32X,18HINITIAL CONDITIONS/5X,20HPOWDER CONDITIONS ---//
114X,8HCALPGM ---//
212.4,6X,8HGASPRS=,F12.4,5H PSI)

```



```

SUM=0.
EKSUM=0.
USQ(1)=U(1,N)**2
DO 300 I=1,IMAX
  EINT(I)=0.
  EKIN(I)=0.
  JMAX=INTERJ(I)-1
  DO 295 J=JMIN,JMAX
    JPLHAF=J
    XI(JPLHAF)=U(J+1,N)**2
    X(J+1,N)=X(J,N)+X(J+1,N))/2.
    EINT(I)=EINT(I)+E(JPLHAF,N)/HALFPO(I)*HALFM(JPLHAF)
    EKIN(I)=(USQ(J)+USQ(J+1))*HALFM(JPLHAF)+EKIN(I)
    EKIN(I)=.5*EKIN(I)
    EINSUM=EINSUM+EINT(I)
    EKIN(6)=.5*EMPROJ*U(JLAST,NMNHAF)**2+EKIN(6)
    EKSUM=EKSUM+EINSUM
    EKSUM=EKSUM+EKIN(I)
    ESUM=EINSUM
    IF(NCHEKE) 301,305,301
    IF(ABS(ETOT-ESUM)-ETENTH) 305,305,302
    EMRNG=1.
    CALL OUTPUT
  IF(JPROJ-400)306,306,307
  JPROJ=300
  TPRINT=T+TMAX
  TNEXT=T+TPRINT
  CALL OUTPUT
  GO TO 121
IF(TNEXT-T) 315,315,121
CALL TOUTPUT+TPRINT
TNEXT=TNEXT+TPRINT
IF(TMAX-TNEXT+.001)320,121,121
TNEXT=TNEXT-TPRINT
TPRINT=OUTDT2
TNEXT=TNEXT+TPRINT
TMAX=5.*TMAX
IF(XSTOP-X(JLAST,NPLUS1)) 556,555,555
CALL OUT
END

```



```

400      GO TO 71
        NYDRA2 = HYDRD2
        IF((NYDRA2.EQ.0).OR.((NYDRA2-60).EQ.0).OR.((NYDRA2-30).EQ.0))
1      GO TO 100
        IF((NYDRA2.GT.30).AND.(NYDRA2.LT.60)) GO TO 300
        IF(NYDRA2.GT.60) GO TO 600
        NZN = 1
        MZM = 1
        INTERJ(NYDRA2 +1) - 1
        GO TO 200
300      NYDRA2 = NYDRA2 -30
        NZN = INTERJ(NYDRA2)
        MZM = INTERJ(NYDRA2+1) -1
        GO TO 200
600      NYDRA2 = NYDRA2 -60
        NZN = INTERJ(NYDRA2)
        MZM = JLAST1
        DO 70 JK = NZN, MZM
            JKM = JK - NZN
            XP6(JKM) = X1(JK)
            VP6(JKM) = U(JK, NMNHAF) / 100.
            XP5(JKM) = X1(JK)
            PP5(JKM) = PPLUSQ(JK)
70      WRITE(M, 7)
100      WRITE(M, 8)
            DO 704 L = 1, JLAST1
            DO 702 IL = 2, ILIMIT
            IF(L - INUE)
702      CONTINUE
            WRITE(M, 4) L, X(L, N), U(L, NMNHAF), V(L, N), PPLUSQ(L), Q(L, NMNHAF),
1      IE(L, N), AREA(L, N), DTSQ(L), X1(L)
            GO TO 704
703      WRITE(M, 5555)
5555      FORMAT(1H )
            WRITE(M, 4) L, X(L, N), U(L, NMNHAF), V(L, N), PPLUSQ(L), Q(L, NMNHAF),
1      IE(L, N), AREA(L, N), DTSQ(L), X1(L)
            CONTINUE
704      WRITE(M, 4) JLAST, X(JLAST, N), U(JLAST, NMNHAF)
71      WRITE(M, 9)
75      WRITE(M, 10) (I, NEQST(I), EKIN(I), EINT(I), I = 1, IMAX)
5      WRITE(M, 5) NCYCLE, T, DTLAST, ESUM
        FORMAT(1H1)
        IF(EMWRCNG) 95, 95, 80
80      WRITE(M, 11)
95      RETURN
40      FORMAT(1I5, 1P7E13.5)

```

```

OUTP0480
OUTP0490
OUTP0500
OUTP0510
OUTP0520
OUTP0530
OUTP0540
OUTP0550
OUTP0560
OUTP0570
OUTP0580
OUTP0590
OUTP0600
OUTP0610
OUTP0620
OUTP0630
OUTP0640
OUTP0650
OUTP0660
OUTP0670
OUTP0680
OUTP0690
OUTP0740
OUTP0750
OUTP0760
OUTP0770
OUTP0780
OUTP0790
OUTP0800
OUTP0810
OUTP0820
OUTP0830
OUTP0840
OUTP0850
OUTP0860
OUTP0870
OUTP0880
OUTP0890
OUTP0900
OUTP0910
OUTP0920
OUTP0930
OUTP0940
OUTP0950
OUTP0960
OUTP0970
OUTP0980
OUTP0990

```



```

1  FORMAT(5X, I2,20H H V MODEL LAUNCHER,4I3)
2  FORMAT(1I8HO J X(J,N) U(J,N-1/2) V(J+1/2,N) P(J+1/2,N) NGUTPI1000
3  1) Q(J+1/2,N-1/2) E(J+1/2,N) AREA(J,N) DTSEC(1/2,1/2) DM(J+1/2,N) NGUTPI1010
4  FORMAT(1I4H BARS-CC/CCO CM/MILLISEC MILLISECSQ GRAMS) NGUTPI1020
5  1  FORMAT(I4,1P6E13.5,2E11.3,E13.5) NGUTPI1030
6  FORMAT(I5,1P3E15.5) NGUTPI1040
7  1) Q(J+1/2,N-1/2) E(J+1/2,N) AREA(J,N) U(J,N-1/2) V(J+1/2,N) P(J+1/2,N) NGUTPI1050
8  FORMAT(1I4H BARS-CC/CCO CM/MILLISEC MILLISECSQ CM ) NGUTPI1060
9  1  FORMAT(46HOREGION MATERIAL K-ENERGY I-ENERGY NGUTPI1070
10  FORMAT(I5,I8, 2E15.5) NGUTPI1080
11  FORMAT(53H1 ENERGY CHECK) NGUTPI1090
12  FORMAT(47HOCYCLE T DT TOTAL E) NGUTPI1100
END NGUTPI1110
NGUTPI1120
NGUTPI1130
NGUTPI1140
NGUTPI1150

```


RETURN
END

CALC0590
CALC0600


```

54      NZONES(IB)=0
      INTERJ(IB)=0
      INTERJ(31)=0
      CALL ZEROA(2,0,PLUSQ,SKIN,TSIGSQ,THETA,VISCO),
      CALL ZEROA(2,0,TMINSQ,TMINSQ,TMINSQ,TMINSQ),
      CALL ZEROA(3,0,VZERO,UZERO,UZERO,UZERO),
      CALL ZEROA(2,0,1,USQ,USQ,USQ),
      CALL ZEROA(2,0,1,X1,X1,X1),
      CALL ZEROB(AREA,200,2)
      CALL ZEROB(AREA,200,2)
      CALL ZEROB(Q,201,2)
      CALL ZEROB(V,200,2)
      CALL ZEROB(P,200,2)
      CALL ZEROB(X,201,2)
      RETURN
      END

```


ZERO0650
ZERO0655
ZERO0660
ZERO0670
ZERO0680
ZERO0690
ZERO0700
ZERO0710
ZERO0720
ZERO0730
ZERO0740
ZERO0750

```
C      SUBROUTINE IERO(I1,I2,I3,I4,I5,I6,I7,I8)
      ZEROS INTEGERS
      I1=0
      I2=0
      I3=0
      I4=0
      I5=0
      I6=0
      I7=0
      I8=0
      RETURN
      END
```

ZERO0760
ZERO0765
ZERO0770
ZERO0780
ZERO0790
ZERO0800
ZERO0810
ZERO0820
ZERO0830
ZERO0840
ZERO0850
ZERO0860

```
C      SUBROUTINE ZERO(Z1,Z2,Z3,Z4,Z5,Z6,Z7,Z8)
      ZEROS NON-INTEGERS
      Z1=0.
      Z2=0.
      Z3=0.
      Z4=0.
      Z5=0.
      Z6=0.
      Z7=0.
      Z8=0.
      RETURN
      END
```

ZERO0870
ZERO0875
ZERO0880
ZERO0890
ZERO0900
ZERO0910
ZERO0920
ZERO0930
ZERO0940
ZERO0950
ZERO0960
ZERO0970

```
C      SUBROUTINE ZEROA(IZA,ZA1,ZA2,ZA3,ZA4,ZA5)
      ZEROS VECTORS
      DIMENSION ZA1(300),ZA2(300),ZA3(300),ZA4(300),ZA5(300)
      DO 1 IZZ=1, IZA
      ZA1(IZZ)=0.
      ZA2(IZZ)=0.
      ZA3(IZZ)=0.
      ZA4(IZZ)=0.
      ZA5(IZZ)=0.
      1 CONTINUE
      RETURN
      END
```

ZERO0980
ZERO0985
ZERO0990
ZERO1000

```
C      SUBROUTINE ZEROB(ZAB,IZA,JZB)
      ZEROS APPAYS
      DIMENSION ZAB (300,10)
      DO 2 IZZ=1, IZA
```



```
DO 1 JZ=1, JZB  
  1 ZAB(IJZ,JZ)=0.  
  2 CONTINUE  
    RETURN  
    END
```

```
ZERO1010  
ZERO1020  
ZERO1030  
ZERO1040  
ZERO1050
```



```

IN60=IN+60
ISTORM(IN10)=NEQST(IN)
ISTORM(IN20)=NZCNEST(IN)
ISTORM(IN)=OUTBDY(IN)
ISTORM(IN10)=OUTGAMMA(IN)
ISTORM(IN20)=COSQX4(IN)
ISTORM(IN30)=UZRO(IN)
ISTORM(IN40)=PO(IN)
ISTORM(IN50)=TO(IN)
ISTORM(IN60)=AMOL(IN)
CONTINUE
STORM(71)=AREA1
STORM(72)=AREA2
STORM(73)=AREA3
STORM(74)=PCGN1
STORM(75)=PCGN2
STORM(76)=SHPRQJ
STORM(77)=EMPTD1
STORM(78)=OUTD1
STORM(79)=TMAX1
STORM(80)=TMAX2
STORM(81)=TMAX3
STORM(82)=XSTOP
STORM(83)=PCGN3
STORM(84)=SLOPE
STORM(85)=RADIUS
STORM(86)=CALPGM
STORM(87)=TURNDR
STORM(88)=GASPR
STORM(89)=R
STORM(90)=EMPIST
STORM(91)=PVWANT
STORM(92)=PVSLEPE
STORM(93)=XPV1
STORM(94)=XPV2
STORM(95)=XPV3
STORM(96)=PVERR
STORM(97)=PRESCG
RETURN
END

```



```

TO      (IN)=STORM(IN50)
1  AMOL  (IN)=STORM(IN60)
    L INUE
    AREA1=STORM(71)
    AREA2=STORM(72)
    AREA3=STORM(73)
    PCOM1=STORM(74)
    PCOM2=STORM(75)
    SHPRCT=STORM(76)
    OUTDT1=STORM(77)
    OUTDT2=STORM(78)
    OUTDT3=STORM(79)
    TMAX1=STORM(80)
    TMAX2=STORM(81)
    XSCN1=STORM(82)
    XSCN2=STORM(83)
    XSCN3=STORM(84)
    SLOPE=STORM(85)
    RADPGND=STORM(86)
    TBUENDR=STORM(87)
    GMSPR=STORM(88)
    GASPR=STORM(89)
    RMP=STORM(90)
    PVS=STORM(91)
    PVS1=STORM(92)
    PVS2=STORM(93)
    XPV1=STORM(94)
    XPV2=STORM(95)
    PVER=STORM(96)
    PRETURN=STORM(97)
    END

```

```

STRE0480
STRE0490
STRE0500
STRE0510
STRE0520
STRE0530
STRE0540
STRE0550
STRE0560
STRE0570
STRE0580
STRE0590
STRE0600
STRE0610
STRE0620
STRE0630
STRE0640
STRE0650
STRE0660
STRE0670
STRE0680
STRE0690
STRE0700
STRE0710
STRE0720
STRE0730
STRE0740
STRE0750
STRE0760
STRE0770
STRE0780
STRE0790

```


RETURN
END

GENS0940
GENS0950


```

902 U(J,NPLHAF)=0.0
903 GO TO 196
904 JPRQJ=5GO
1755 DTSQ(200)=T
      IF(J.EQ.JMAX.AND.NZN.EQ.1) GO TO 876
      IF(J.EQ.JMAX.AND.NZN.GT.1) GO TO 800
      DUDT=(PPLUSQ(JMNHAF)-PPLUSQ(JPLHAF))*AREA(J,N)/(HALFM(JMNHAF)+
1      HALFM(JPLHAF))
      GO TO 195
800 IF(J.EQ.INTERJ(6)) GO TO 863
      DUDT=-1.5*(PPLUSQ(JPLHAF)-PPLUSQ(JMNHAF))-(PPLUSQ(JPLHAF+1)-
1      PPLUSQ(JMNHAF-1))/6.)*AREA(J,N)/(HALFM(JMNHAF)+HALFM(JPLHAF))
      GO TO 195
863 DUDT=-1.5*(PPLUSQ(JPLHAF)-PPLUSQ(JMNHAF))-(PPLUSQ(JPLHAF+1)-
1      (PPLUSQ(JMNHAF)/3.+2.*PPLUSQ(JMNHAF-1)/3.
1      )/6.)*AREA(J,N)/(HALFM(JMNHAF)+HALFM(JPLHAF))
      GO TO 194
194 IF(T.GE.(DTSQ(200)+DTSQ(199))) GO TO 194
      DUDT=DUDT*(T-DTSQ(200))/DTSQ(199)
      CONTINUE
      GO TO 195
876 A=2.*HALFM(JMNHAF)
      B=HALFM(JMNHAF)+HALFM(JPLHAF)
      DUDT=((2.*A**2*(A+B)*PPLUSQ(JPLHAF))
1      -((2.*A-B)*(A+B)*PPLUSQ(JMNHAF-1))/(A*(A+B)*B)*(-1.)*AREA(J,N)
2      +(A-B)*B*PPLUSQ(JMNHAF)+DTMIN(NN)*DUDT
195 U(J,NPLHAF)=U(J,NMNHAF)+DTMIN(NN)*DUDT
196 X(J,NPLUS1)=X(J,N,NPLHAF)
      CALL ARCOMP
      CALL VCCOMP
      V(JMNHAF,NPLUS1)=HALFRO(I)/HALFM(JMNHAF)*VOLUME
200 IF(U(J,NPLHAF)-U(J-1,NPLHAF)) 205,225,225
205 Q(JMNHAF,NPLHAF)=CQSQX4(I)*HALFRO(I)*{U(J,NPLHAF)-U(J-1,NPLHAF)}
1      I**2/(V(JMNHAF,NPLUS1)+V(JMNHAF,N))
      GO TO 230
225 Q(JMNHAF,NPLHAF)=0.
230 INDEX=NEQST(I)
      IF(INDEX.EQ.1) CALL EQST1
      IF(INDEX.EQ.2) CALL EQST2
      IF(INDEX.EQ.3) CALL EQST3
53 DO 240 J=JMIN,JMAX
      JMNHAF=J-1
      IF(JPRQJ.LT.300.AND.J.GT.INTERJ(6)) GO TO 24
      TSIGSQ(JMNHAF)=CSQ(JMNHAF)/(X(J,NPLUS1)-X(J-1,NPLUS1))**2
      CCNTINUE
      PPLUSQ(JMNHAF)=P(JMNHAF,NPLUS1)+Q(JMNHAF,NPLHAF)
24 DLAMCA(JMNHAF)=CQSQX4(I)/2.*(V(JMNHAF,N
1      (V(JMNHAF,N)+V(JMNHAF,NPLUS1))
      )-V(JMNHAF,NPLUS1))/

```



```

DLAMAX = MAX1(DLAMDA(JMNHAF),DLAMAX)
SIGMAX = MAX1(TSIGSQ(JMNHAF),SIGMAX)
CSQMAX = MAX1(CSQMAX,CSQ(JMNHAF))
IF (TSIGSQ(JMNHAF) .NE. 0.0) GO TO 240
DTSQ(JMNHAF) = 0.0
GO TO 245
240 DTSQ(JMNHAF) = .111111/TSIGSQ(JMNHAF)
245 CMAXR(I) = SQR T(CSQMAX)
340 CONTINUE
246 RETURN
END

```

```

DYNM0940
DYNM0950
DYNM0960
DYNM0970
DYNM0980
DYNM0990
DYNM1000
DYNM1010
DYNM1020
DYNM1030
DYNM1040

```



```
16 VOLUME=(X(J,NPLUS1)-X(J-1,NPLUS1))*AREA3  
17 RETURN  
END
```

VCOM0530
VCOM0540


```

C CAL SUBROUTINE EQST1
COMMON PCON3, SLOCPE, AND ENERGY FOR IDEAL GAS ZONES
1, DPMU, Q1, DQ2, DS, AREA2, AREA3, CALPGM, TBURNND, GMSPDR, GASPRS, IHEL, CV, DLAMAX,
2, EWFONG, E1, FCRCE, TDT2, DS, EZER, HALFM, PCON2, TVFREQ, UZER, U, USQ, XMAX, Z, MASS, EMP, RCJ, XSTCP,
3, SIGMAX, SIGMIN, T, VNEXT, T, VCLUME, VISCOS, X, X1, XGRID, XMIN, XMAX, Z, MASS, EMP, RCJ, XSTCP,
4, PRINT, T, VNEXT, T, VCLUME, VISCOS, X, X1, XGRID, XMIN, XMAX, Z, MASS, EMP, RCJ, XSTCP,
5, VZERO, V, VCLUME, VISCOS, X, X1, XGRID, XMIN, XMAX, Z, MASS, EMP, RCJ, XSTCP,
6, COMMON, IMAX, INU, I, IT, JLAST, JLAS, ILIMAX, JPRD, J1, JPRD, J2, JMIN, JMAX, J,
7, JPLHAF, JMNHAF, J, JLAST, JLAS, ILIMAX, JPRD, J1, JPRD, J2, JMIN, JMAX, J,
1, JPLHAF, JMNHAF, J, JLAST, JLAS, ILIMAX, JPRD, J1, JPRD, J2, JMIN, JMAX, J,
2, JPLHAF, JMNHAF, J, JLAST, JLAS, ILIMAX, JPRD, J1, JPRD, J2, JMIN, JMAX, J,
3, JPLHAF, JMNHAF, J, JLAST, JLAS, ILIMAX, JPRD, J1, JPRD, J2, JMIN, JMAX, J,
4, JPLHAF, JMNHAF, J, JLAST, JLAS, ILIMAX, JPRD, J1, JPRD, J2, JMIN, JMAX, J,
5, JPLHAF, JMNHAF, J, JLAST, JLAS, ILIMAX, JPRD, J1, JPRD, J2, JMIN, JMAX, J,
6, JPLHAF, JMNHAF, J, JLAST, JLAS, ILIMAX, JPRD, J1, JPRD, J2, JMIN, JMAX, J,
7, JPLHAF, JMNHAF, J, JLAST, JLAS, ILIMAX, JPRD, J1, JPRD, J2, JMIN, JMAX, J,
DO 10 JMNHAF=JMIN1, JMAX1
E1=E(JMNHAF, N)-(P(JMNHAF, N)+Q(JMNHAF, NPLHAF))* (V(JMNHAF, NPLUS1)-
1 V(JMNHAF, N))
P1=E1*(GAMMA(I)-1.0)/ V(JMNHAF, NPLUS1)-
E(JMNHAF, N)
1 V(JMNHAF, N)
P(JMNHAF, NPLUS1)=E(JMNHAF, NPLUS1)*(GAMMA(I)-1.0)/ V(JMNHAF, NPLUS1)
CSQ(JMNHAF)=GAMMA(I)*(GAMMA(I)-1.0)*E(JMNHAF, NPLUS1)/ROZERO(I)
RETURN
END

```

10

INPUT FORMAT

CARD 1 (4I3,F10.0)

IDATA = 0, STANDARD 18 CARD INPUT
 = 1, NAMELIST INPUT OF ALL VARIABLES ON CARDS
 IPRNTZ = 0, STANDARD RUN
 = 1, PRINT OUT INITIAL DATA ONLY
 INTRNSF = 0, USE DISK SCRATCH FILE AND PRINTOUT ONLY LAST PISTON
 = 1, PRINT OUT ALL PISTON ITERATIONS (HYPERVELOCITY MODEL ONLY)
 IPUNCH = 0, NO PUNCHED OUTPUT
 = 1, PUNCHED OUTPUT OF MODEL BASE PRESSURE VS TIME
 DTSQ(199) FINITE BREAK VALVE OPENING TIME

CARD 2 (20I3)

IMAX = NUMBER OF REGIONS (UP TO SIX)
 NCATE1 = MONTH
 NCATE2 = DAY
 NCATE3 = YEAR
 NUMBER = RUN IDENTIFICATION NUMBER
 NCHEKE = 0, NO ENERGY CHECK
 = 1, ENERGY MONITORED AND PROBLEM STOPPED IF THE TOTAL ENERGY
 CHANGES BY MORE THAN 10%
 INU = 0, ALL ZONES HAVE ZERO INITIAL VELOCITY
 = 1, ALLOWS INITIAL VELOCITY FOR EACH ZONE TO BE READ
 JPROJ = MASS POINT NUMBER OF PROJECTILE

CARD 3 (2013)
 NEQST(I) = NUMBER OR INDEX OF EQUATION OF STATE USED IN REGION I

CARD 4 (2013)
 NZONES(I) = NUMBER OF ZONES IN REGION I

CARD 5 (7F10.0)
 OUTBDY(I) = DISTANCE IN CM TO OUTER INTERFACE OF REGION I

CARD 6 (7F10.0)
 GAMMA(I) = RATIO OF SPECIFIC HEATS FOR REGION I

CARD 7 (7F10.0)
 CQSXQ4(I) = CONSTANT USED IN ARTIFICIAL VISCOSITY COMPUTATION (GOOD
 VALUES ARE 4.0 FOR GAS REGION, 9.0 FOR SOLID REGION)

CARD 8 (7F10.0)
 AREA1 = AREA IN SQ CM OF FIRST CONSTANT AREA SECTION (PROGRAM ALLOWS UP TO
 THREE DIFFERENT CONSTANT AREA SECTIONS AND ONE TAPERED SECTION
 BETWEEN THE SECOND AND THIRD CONSTANT AREA SECTIONS)
 AREA2 = AREA IN SQ CM OF SECOND CONSTANT AREA SECTION
 AREA3 = AREA IN SQ CM OF THIRD CONSTANT AREA SECTION
 PCON1 = POSITION IN CM WHERE FIRST AREA CHANGE OCCURS
 PCON2 = POSITION IN CM WHERE SECOND AREA CHANGE OCCURS
 SHPR = PROJECTILE RELEASE PRESSURE IN BARS
 EMPROJ = MASS OF PROJECTILE IN GRAMS

OUTDT1 = DELTA T FOR PRINTING UP TO TIME TMAX1
 TMAX1 = MILLISECS
 OUTDT2 = DELTA T FOR PRINTING UP TO TIME TMAX2
 TMAX2 = MILLISECS
 XSTOP = POSITION IN CM THAT WHEN THE INTERFACE JSTOP REACHES IT,
 THE PROBLEM IS TERMINATED

CARD 9 (7F10.0) REQUIRED ONLY IF INU = 1
 UZERO(I) = INITIAL VELOCITY FOR EACH ZONE

CARD 10 (7F10.0)
 PCON = POSITION IN CM WHERE THIRD AREA CHANGE OCCURS
 SLOPE = SLOPE OF CONSTANT TAPERED SECTION
 RADIUS = RADIUS IN CM OF THE CONSTANT AREA SECTION TO THE RIGHT
 OF THE TAPERED SECTION

CARD 11 (4F10.0,I4)
 CALPGM = CALORIES PER GRAM OF POWDER
 TBURND = TIME TO BURN POWDER
 GMSPDR = GRAMS OF POWDER
 GASPRS = INITIAL GAS PRESSURE IN POWDER REGION
 IHEL= 0 (NOT APPLICABLE TO GUN PROJECT)


```

CARD 12 (7F10.0)
      IPOX = 0  ALL PLOTS, ALL PRESSURE POINTS (PLOT ROUTINE MUST BE INCLUDED)
            = 1  ALL PLOTS, NO PRESSURE POINTS
            = 5  NO PLOTS, NO PRESSURE POINTS
            = 6  ONLY PRESSURE POINTS

      NPOX = NUMBER OF PRESSURE POINTS (UP TO FIVE)
      XPO(I) = X POSITION IN CM OF PRESSURE POINT I

CARD 13 (7F10.0)  HYPERVELOCITY MODEL LAUNCHER PARAMETERS, (NOT APPLICABLE
                   TO GUN PROJECT)

      XPV1 = X POSITION IN CM OF FIRST MEASUREMENT POINT OF PISTON VELOCITY
      XPV2 = X POSITION IN CM OF SECOND MEASUREMENT POINT OF PISTON VELOCITY
      PVERR = PISTON VELOCITY ERROR IN FT PER SEC
      PVWANT = DESIRED PISTON VELOCITY IN FT PER SEC

CARD 14 (E10.0,3F10.0)

      R = .8317E 08      GAS CONSTANT
      EMPIST = MASS OF FIRST PISTON SECTION ( HYPERVELOCITY MODEL LAUNCHER ONLY)
      FRAC = 1.0
      EMLEAD = MASS OF SECOND PISTON SECTION (HYPERVELOCITY MODEL LAUNCHER)

CARD 15 (7F10.0)

      PO(I) = INITIAL PRESSURE IN PSI IN REGION I

CARD 16 (7F10.0)

      TO(I) = INITIAL TEMPERATURE IN DEGREES KELVIN IN REGION I

```


CARD 17 (7F10.0)

AMOL(I) = MOLECULAR WEIGHT OF MATERIAL IN REGION I

CARD 18 (I3)

ILASTK = 0; STOP
 = 1; CONTINUE FOR NEW RUN

LIST OF REFERENCES

1. Oertel, F. H. Jr., "Investigations of Transitional Ballistics in a Muzzle Jet Flow Simulator," Proceedings of the First International Symposium on Ballistics, Orlando, Florida, November, 1974.
2. Schroder, G.A. and Klingenberg, C., "Investigation of Flow Phenomena Associated with the Muzzle Flash of Small Caliber Guns," Proceedings of the First International Symposium on Ballistics, Orlando, Florida, November, 1974.
3. Maillie, F. H., "Projectile Environment During Intermediate Ballistics," Proceedings of the First International Symposium on Ballistics, Orlando, Florida, November, 1974.
4. Collier, R., Burckhardt, C.B., and Lin, L.H., Optical Holography, Academic Press, New York, 1971.
5. Everett, R.A., Experimental Techniques in Holographic Interferometry, Masters Thesis, Naval Postgraduate School, Monterey, Ca., 1973.
6. Floyd, R.P. and Collins, D.J., "Holographic Determination of Simple Translation and Rotations," American Journal of Physics, v. 39/4, p. 359-362, April, 1971.
7. Jones, H.W., Application of Holographic Interferometry to Supersonic Flow Visualization of a Rear-Facing Step and Application of Fast Fourier Transform Methods to Current Data Reduction Techniques, Masters Thesis, Naval Postgraduate School, Monterey, Ca., 1974.
8. Naval Ordnance Laboratory Technical Report 62-87, Ballistics Research Report 67, 1963, Computer Analysis of Two-Stage Hypervelocity Model Launchers, by R. Piacesi, D.F. Gates, and A.E. Seigel.
9. Richtmyer, R.D., Difference Methods for Initial Value Problems, Interscience Publishers, Inc., New York, 1957.
10. Streeter, V.L., Fluid Mechanics, McGraw-Hill, 1971.

11. Advisory Group for Aerospace Research and Development (NATO) Publication No. AGARD-AG-186, Laser Instrumentation for Flow Field Diagnostics, by J.D. Trolinger, March, 1974.
12. Van Dyke, M.D., "The Supersonic Blunt Body Problem-Review and Extension," J. Aero/Space Sci., v. 25, p. 485-495, 1958.
13. Van Neumann, I. and Richtmyer, R.D., "A Method for Numerical Calculation of Hydrodynamic Shocks," Journal of Applied Physics, v. 21, p. 232, 1950.

INITIAL DISTRIBUTION LIST

	No. Copies
1. Defense Documentation Center Cameron Station Alexandria, Virginia 22314	2
2. Library, Code 0212 Naval Postgraduate School Monterey, California 93940	2
3. Chairman, Department of Aeronautics Naval Postgraduate School Monterey, California 93940	1
4. Professor D. J. Collins Department of Aeronautics Naval Postgraduate School Monterey, California 93940	3
5. LT R. G. Bettinger, USN 2850 West Dale N.W. Canton, Ohio 44708	2
6. Professor D. W. Netzer Department of Aeronautics Naval Postgraduate School Monterey, California 93940	1
7. Mr. Michael Lamb Naval Ordnance Station, Code 50326 Indian Head, Maryland 20640	2

Thesis

160542

B4595

Bettinger

c.1

Application of holo-
graphic interferometry
to the exterior bal-
listic flow field in
the muzzle environment
of a twenty millimeter
cannon.

Thesis

160542

B4595

Bettinger

c.1

Application of holo-
graphic interferometry
to the exterior bal-
listic flow field in
the muzzle environment
of a twenty millimeter
cannon.

Application of holographic interferometr



3 2768 002 13792 9

DUDLEY KNOX LIBRARY